National Library of Canada
Bibliothèque nationale du Canada

Canadian Theses Service
Service des thèses canadiennes

Ottawa, Canada
K1A 0N4

NOTICE

The quality of this microform is heavily dependent upon the quality of the original thesis submitted for microfilming. Every effort has been made to ensure the highest quality of reproduction possible.

If pages are missing, contact the university which granted the degree.

Some pages may have indistinct print especially if the original pages were typed with a poor typewriter ribbon or if the university sent us an inferior photocopy.

Reproduction in full or in part of this microform is governed by the Canadian Copyright Act, R.S.C. 1970, c. C-30, and subsequent amendments.

AVIS

La qualité de cette microforme dépend grandement de la qualité de la thèse soumise au microfilmage. Nous avons tout fait pour assurer une qualité supérieure de reproduction.

S'il manque des pages, veuillez communiquer avec l'université qui a conféré le grade.

La qualité d'impression de certaines pages peut laisser à désirer, surtout si les pages originales ont été dactylographiées à l'aide d'un ruban usé ou si l'université nous a fait parvenir une photocopie de qualité inférieure.

La reproduction, même partielle, de cette microforme est soumise à la Loi canadienne sur le droit d'auteur, SRC 1970, c. C-30, et ses amendements subséquents.

NL-339 (r. 88/04) c

Canada

UNIVERSITY OF ALBERTA

COMPARATIVE EVAPOTRANSPIRATION MEASUREMENTS AND THE CANOPY RESISTANCE OF AN ALFALFA FIELD

by

WILLIAM L. MAYNARD (C)

A THESIS

SUBMITTED TO THE FACULTY OF GRADUATE STUDIES AND RESEARCH

IN PARTIAL FULFILMENT OF THE REQUIREMENTS FOR THE DEGREE

OF MASTER OF SCIENCE

IN

METEOROLOGY

DEPARTMENT OF GEOGRAPHY

EDMONTON, ALBERTA

FALL, 1990

National Library of Canada
Bibliothèque nationale du Canada

Canadian Theses Service
Service des thèses canadiennes

Ottawa, Canada
K1A 0N4

The author has granted an irrevocable non-exclusive licence allowing the National Library of Canada to reproduce, loan, distribute or sell copies of his/her thesis by any means and in any form or format, making this thesis available to interested persons.

L'auteur a accordé une licence irrévocable et non exclusive permettant à la Bibliothèque nationale du Canada de reproduire, prêter, distribuer ou vendre des copies de sa thèse de quelque manière et sous quelque forme que ce soit pour mettre des exemplaires de cette thèse à la disposition des personnes intéressées.

The author retains ownership of the copyright in his/her thesis. Neither the thesis nor substantial extracts from it may be printed or otherwise reproduced without his/her permission.

L'auteur conserve la propriété du droit d'auteur qui protège sa thèse. Ni la thèse ni des extraits substantiels de celle-ci ne doivent être imprimés ou autrement reproduits sans son autorisation.

ISBN 0-315-65075-3

UNIVERSITY OF ALBERTA

RELEASE FORM

NAME OF AUTHOR: WILLIAM L. MAYNARD

TITLE OF THESIS: COMPARATIVE EVAPOTRANSPIRATION MEASUREMENTS AND THE CANOPY RESISTANCE OF AN ALFALFA FIELD

DEGREE: MASTER OF SCIENCE

YEAR THIS DEGREE GRANTED: 1990

PERMISSION IS HEREBY GRANTED TO THE UNIVERSITY OF ALBERTA LIBRARY TO REPRODUCE SINGLE COPIES OF THIS THESIS AND TO LEND OR SELL SUCH COPIES FOR PRIVATE, SCHOLARLY OR SCIENTIFIC RESEARCH PURPOSES ONLY.

THE AUTHOR RESERVES OTHER PUBLICATION RIGHTS, AND NEITHER THE THESIS NOR EXTENSIVE EXTRACTS FROM IT MAY BE PRINTED OR OTHERWISE REPRODUCED WITHOUT THE AUTHOR'S WRITTEN PERMISSION.

(SIGNED) Bill Maynard

PERMANENT ADDRESS:

Box 1106
Nanton, Alberta
TOL 1R0

DATED: July 27, 1990

THE UNIVERSITY OF ALBERTA

FACULTY OF GRADUATE STUDIES AND RESEARCH

The undersigned certify that they have read, and recommend to the Faculty of Graduate Studies and Research for acceptance, a thesis entitled COMPARATIVE EVAPO-TRANSPIRATION MEASUREMENTS AND THE CANOPY RESISTANCE OF AN ALFALFA FIELD submitted by WILLIAM L. MAYNARD in partial fulfilment of the requirement for the degree of MASTER OF SCIENCE in METEOROLOGY.

J. D. Wilson, Supervisor

R. B. Charlton

D. S. Chanasyk

Date: March 29, 1990

ABSTRACT

A field comparison of three different methods for measuring the latent heat flux was conducted in the summer of 1988. The methods included two variations of the eddy correlation approach involving sensing the temperature, humidity and vertical velocity fluctuations of the eddies, and a Bowen ratio method using instrumentation assembled for this study. The results of the field season are provided along with the requisite background theory necessary to understand both the operating principles of the instrumentation and the manipulation of data used to obtain the final results. The evaporation data are used to estimate the bulk stomatal resistance (canopy resistance) to transpiration from the local alfalfa canopy, and these results are compared to those obtained in similar studies found in the literature. Conclusions are drawn about the performance of the three techniques used for estimating evapotranspiration and the utility of the data derived from it.

ACKNOWLEDGEMENTS

I especially wish to thank my supervisor, Dr. John Wilson, and meteorology secretary, Laura Smith, for their assistance and encouragement during this research. I also wish to thank Peter Dzikowski of Alberta Agriculture and Research Meteorologist, Ken Stewart of the Canadian Forces Forecast Centre, Edmonton for their help and support.

To my parents, for their love, devotion and confidence in me, I am truly grateful.

TABLE OF CONTENTS

CHAPTER		PAGE
I	EVAPOTRANSPIRATION THEORY.	1
	1.1. Introduction	1
	1.2. The Energy Balance	2
	1.3. Micrometeorological Determination. . . .	4
	1.4. Models	7
	1.5. Objectives	10
II	THE EXPERIMENT	12
	2.1. Field Site	12
	2.2. Instrumentation.	14
	2.3. Bowen Ratio Device	14
	2.4. Sonic Anemometer	21
	2.5. Fine Wire Thermocouple	24
	2.6. Net Radiometer	24
	2.7. Soil Heat Flux Plate	25
	2.8. Lyman-α Humidiometer	25
	2.9. Ancillary Equipment.	26
III	FIELD RESULTS.	29
	3.1. Energy Balances.	29
	3.2. Comparative Latent Heats	41
	3.3. Failure to Close Energy Balance.	53
	3.4. Estimate of Soil Heat Flux Error	58
	3.5. Canopy Resistances	59
IV	CONCLUSIONS.	72
BIBLIOGRAPHY		74
APPENDIX 1		77
APPENDIX 2		81

LIST OF TABLES

		Page
Table 1	Daily result summaries.....	42
Table 2	Horizontal arm Bowen ratio results.....	57

LIST OF FIGURES

FIGURE		PAGE
1.	Sketch of reversing psychrometer arm	19
2.	Sketch of psychrometer sensors.....	20
3.	Sketch of reversing motor mount.....	22
4.	Sketch of motor control circuit.....	23
5.	Calibration curves for humidiometer.....	27
6.	Energy balance May 15, 1988.....	30
7.	Energy balance May 16, 1988.....	31
8.	Energy balance May 17, 1988.....	32
9.	Energy balance May 18, 1988.....	33
10.	Energy balance May 19, 1988.....	34
11.	Energy balance May 20, 1988.....	35
12.	Energy balance May 21, 1988.....	36
13.	Energy balance June 2, 1988.....	37
14.	Energy balance June 14, 1988.....	38
15.	Energy balance June 15, 1988.....	39
16.	Energy balance June 23, 1988.....	40
17.	Comparative latent heats May 15, 1988.....	43
18.	Comparative latent heats May 16, 1988.....	44
19.	Comparative latent heats May 17, 1988.....	45
20.	Comparative latent heats May 18, 1988.....	46
21.	Comparative latent heats May 19, 1988.....	47
22.	Comparative latent heats May 20, 1988.....	48
23.	Comparative latent heats May 21, 1988.....	49
24.	Comparative latent heats June 2, 1988 with accompanying windspeed plot.....	50

List of Figures, continued:

FIGURE		PAGE
25	Comparative latent heats June 14, 1988 with accompanying windspeed plot.....	51
26	Comparative latent heats June 23, 1988.....	52
27	Absolute and relative sensible heats.....	56
28	Canopy resistance May 15, 1988.....	60
29	Canopy resistance May 16, 1988.....	61
30	Canopy resistance May 17, 1988.....	62
31	Canopy resistance May 18, 1988.....	63
32	Canopy resistance May 19, 1988.....	64
33	Canopy resistance May 20, 1988.....	65
34	Canopy resistance May 21, 1988.....	66
35	Canopy resistance June 2, 1988.....	67
36	Aerodynamic resistance for June 2, 1988 with accompanying windspeed plot.....	69
37	Daily canopy resistance and rainfall.....	71

LIST OF PHOTOGRAPHIC PLATES

		Page
Plate 1.	Photograph of field site and instrumentation.....	13
Plate 2.	Photograph of reversing psychrometer apparatus.....	17

LIST OF SYMBOLS

A	area, m^2
B	Bowen ratio
C_p	heat capacity at constant pressure, J kg^{-1} K^{-1}
d	measuring path length, m
D	damping depth, m
e	ambient vapour pressure, Pa
e_s	saturation vapour pressure, Pa
E	vapour flux density, kg m^{-2} s^{-1}
f	frequency, s^{-1}
I	current, Amps
I_o	discharge current, Amps
k	von Karmen's constant, 0.40
L	latent heat of vapourization, 2.5 x 10^6 J kg^{-1}
m_v	mass of vapour, kg
N	integer
Q_E	latent heat flux density, W m^{-2}
Q_G	soil heat flux density, W m^{-2}
Q_H	sensible heat flux density, W m^{-2}
Q_H'	sensible heat flux density for absolute temperature eddy correlation, W m^{-2}
Q^*	net heat flux density, W m^{-2}
r_a	aerodynamic resistance, s m^{-1}
r_c	"canopy" resistance, s m^{-1}
r_H	transfer resistance to sensible heat, s m^{-1}

List of Symbols, continued:

r_v	transfer resistance to latent heat, s m^{-1}
R_v	gas constant for water vapour, J kg^{-1} K^{-1}
S	slope of saturation vapour pressure curve, Pa h^{-1}
t	time, s
T	temperature, K
T_w	wet bulb temperature, K
T'	fluctuation in temperature, T'
u	windspeed, m s^{-1}
u_*	friction velocity, m s^{-1}
V	volume m^3 or Volts
z	height, m
z_o	roughness length, m
z_s	screen height, m
w	vertical velocity, m s^{-1}
w'	fluctuation in vertical velocity, m s^{-1}
μ	absorption coefficient (Lyman-α)
γ	psychrometric constant, Pa K^{-1}
ρ	density, kg m^{-3}
ρ_v	absolute humidity, kg m^{-3}
ρ_v'	fluctuation of absolute humidity, kg m^{-3}
ω	angular velocity, radians s^{-1}
κ	diffusivity, m^2 s^{-1}
λ	wavelength, m

CHAPTER I

EVAPOTRANSPIRATION THEORY

1.1. Introduction

Evapotranspiration from vegetated surfaces may be measured using a variety of techniques, and the data gained from such measurements may be analyzed to determine several micrometeorological variables and their associated diurnal variation. There are two micro-meteorological approaches to measuring the vertical water vapour flux. First, the direct eddy correlation method which requires sensing the vertical velocity and humidity fluctuations on an instantaneous basis, and second, profile methods which deduce the flux from averaged differences in atmospheric properties between two fixed levels. There are, in addition, non-meteorological approaches which measure the moisture loss from the soil using, for example, lysimeters or neutron moisture meters. There are also numerous empirical formulae. Many of the methods used for finding the evapotranspiration can also be used to determine the energy partition and other variables, such as "canopy resistance", with appropriate instrumentation

and related theory. The results are of interest to hydrologists, climatologists, botanists, and agronomists, among others.

1.2. The Energy Balance

The incoming and outgoing energy fluxes at the earth's surface must balance if there is to be no net gain of energy at the surface over time. This assumption is referred to as the energy balance. Normally, the largest factor in the balance is the net radiation, Q^*, which is the net rate of gain or loss of radiative energy at a surface. The net radiative flux is equal to the amount of solar energy incident at the surface (assumed horizontal) from the sun plus the long-wave (terrestrial) flux originating from the atmosphere minus the reflected solar flux and the outgoing terrestrial radiative flux. By convention, the flux is defined as positive when the incoming energy exceeds the outgoing energy.

Part of the radiative energy surplus is transferred to the atmosphere via an upward turbulent convective flux of sensible heat, Q_H, and the quantity that is used for evaporation is referred to as the latent heat flux, Q_E. The latent heat flux is positive when energy is being consumed to support evaporation, and is negative for condensation. The sensible heat flux is positive

when the air is gaining energy. The Bowen ratio is defined as:

$$B = \frac{Q_H}{Q_E} \tag{1}$$

The final heat flux of significance is the soil heat flux, Q_G. This is a measure of the amount of energy going into soil storage and is defined as positive when heat is being gained by the soil. The primary means of energy transfer through the soil is conduction, whereas that for latent and sensible heat is turbulent convection.

A complete energy balance would include terms for photosynthesis and the storage of heat in the ground and in the vegetated canopy; however, for our purposes, it is sufficient to equate the net radiative flux with the three other fluxes so that:

$$Q^* = Q_H + Q_E + Q_G \tag{2}$$

As the morning progresses and the net radiant flux increases, so will the sum of the other heat fluxes rise in response. Although the sum will always rise and fall in response to the net radiant flux, the individual fluxes will not always vary proportionately. For example, Q_E may fall rapidly later in the day as plant tissue water is depleted and plant stomates close in response to that

stress; Q_H will rise to compensate. On most clear days, though, the energy associated with each flux increases with increasing net radiation with a notable delay in the soil heat flux peak relative to the others due to the thermal inertia of the soil.

In the evening or at night when the net energy flux is negative, the values of these fluxes will continue to balance though the energy is being transferred in the opposite sense. To elaborate by example, the outgoing net radiation will equal the amount of heat being lost due to atmospheric cooling, condensation, or continued evaporation (depending on the atmospheric vapour pressure and the nature of the underlying surface) and soil cooling.

1.3. Micrometeorological Determination of Evapotranspiration

Micrometeorological methods of estimating the latent heat flux always involve an assumption of symmetry. When symmetry is valid the mean vapour flux passing through an elevated plane parallel to the surface is identical to the vapour flux at the surface. The conditions that must be satisfied for this assumption to hold true are that there be no change in the storage of vapour between the surface and the plane and that

there be horizontal uniformity of the lateral heat flux. These ideals are most closely matched far from the upwind edge of a large uniformly vegetated field (i.e., with a long undisturbed upwind path length or "fetch").

The assumption of symmetry allows an intuitive definition of the evaporative flux. For simplicity, consider the transport of vapour through an imaginary thin slab of the atmosphere lying parallel to the ground. This slab is thin enough that no significant changes in the absolute humidity of the air will occur in the time it takes for the air to move through it.

The time, Δt, required for the air to travel upwards through this slab will be brief enough that the vertical velocity, w, will be constant. The thickness of the slab, Δz, can then be closely approximated by multiplying the time period, Δt, required to traverse the latter by the vertical velocity of the air moving through it. If we consider an arbitrary area of the slab, A, then the volume of air, V, moving through it during that time will be:

$$V = w \Delta t A \qquad (3)$$

The mass of water vapour within that volume would then be:

$$m_v = \rho_v V = \rho_v w \Delta t A \quad (4)$$

where ρ_v is the absolute humidity of the air, the mass of water vapour per unit volume (kg m^{-3}).

The rate of passage of vapour through the plane, E, at height, z, per unit time would then be:

$$E = \frac{\rho_v w \Delta t A}{\Delta t A} = \rho_v w \quad (5)$$

Due to the turbulent nature of the atmosphere these quantities must be measured frequently and averaged over a suitably long period of time in order to provide useful estimates of the mean local flux. That is, for practical applications it is necessary to measure:

$$\bar{E}(z) = \frac{1}{N} \sum_{i=1}^{N} w_i \rho_{vi} = \overline{w\rho_v} \quad (6)$$

This equation is the basis of the Eddy correlation method for measuring evaporation. The correlation comes about because in general, though not always, upward moving air will, by day, be carrying relatively moist parcels upwards, whereas downward moving air will be carrying relatively drier air from above.

By following similar arguments, the sensible heat flux density can be shown to be:

$$Q_H = \rho C_p \frac{1}{N} \sum_{i=1}^{N} w_i T_i = \rho C_p \overline{wT} \quad (7)$$

In practise these eddy fluxes are measured and evaluated using:

$$Q_H = \rho C_p \overline{wT} = \rho C_p (\overline{wT} - \bar{w}\,\bar{T}) \quad (8)$$

and

$$Q_E = L \overline{w\rho_v} = L (\overline{w\rho_v} - \bar{w}\,\bar{\rho}_v) \quad (9)$$

where in theory, though not always in practise due to instrumental or site limitations; $\bar{w} = 0$.

Note that the moisture flux at the surface (i.e., the desired quantity E_o) will not necessarily equal the measured flux (through a plane above the surface) if moisture is advecting over the field from an adjacent area (i.e., if the symmetry requirement is not met).

1.4. Models

Many models of evapotranspiration are available, ranging from crude correlations against temperature and sunshine hours (etc.), through models paying some respect to physical principles, to extremely detailed treatments of the entire canopy microclimate, including calculation of the radiative divergence of the canopy and the

individual leaf energy balance for a representative set of canopy layers (Naot and Mahrer, 1986).

In this thesis the focus will be placed on the Monteith "big leaf" model, a fairly simple but nontheless physically insightful model that treats an entire canopy as one big leaf. This model is derived from the principle of energy conservation and the Ohm's law analogy for the turbulent convective fluxes and is given by (Monteith, 1965):

$$Q_E = \frac{S(Q^* - Q_G) + \rho C_p (e_s(T) - e)\, r_a^{-1}}{S + \gamma + \gamma\, r_c r_a^{-1}} \qquad (10)$$

where e and T are vapour pressure and temperature measured at some reference level (say, "screen" height), S is the slope of the saturation vapour pressure curve, and γ is the psychrometric "constant". The r's are transfer resistances. Considering the "big leaf" as a source for heat and vapour which travel down a diffusion pathway to the reference level, there is clearly a greater resistance to vapour loss than heat loss, since the vapour must pass through the stomata. The canopy resistance r_c represents in the model this additional resistance to vapour loss, and the remaining resistance (which consists of boundary-layer and aerodynamic resistance and is treated as being equal for heat and vapour diffusion) is r_a. According to Thom (1972) the aerodynamic resistance in neutral strati-

fication is:

$$r_a = \frac{\bar{u}(z_s)}{u_*^2} + 6.266\, u_*^{-2/3} \qquad (11)$$

where the friction velocity u_* and the reference velocity $\bar{u}(z_s)$ must be specified in m s^{-1}. Van Zyl and De Jager (1987) have shown that stability effects on r_a are small. Therefore, we need only $\bar{u}(z_s)$ and u_* to determine the aerodynamic resistance. We have neglected the influence of stability on the shape of the wind profile and have simply used the logarithmic wind profile:

$$\bar{u}(z) = \frac{u_*}{k} \ln \frac{z}{z_o} \qquad (12)$$

where k is von Karman's constant which has been experimentally found to be 0.40, and z_o is the roughness length which is a measure of the aerodynamic roughness of the surface. It follows that u_* is given by the slope of the wind profile:

$$u_* = k \frac{\Delta u}{\Delta \ln z} \qquad (13)$$

The canopy resistance is a bulk measure of the stomatal resistance of the crop as a whole and is in reality not uniquely controlled by the individual leaf stomatal resistance. The transpiration rate of a plant

is controlled by the variable-aperture stomates on one or both sides of the plant's surface. These stomates are porous openings representing 0.3% to 1.0% of the leaf area when fully open (Rutter, 1975). When the plant is under moisture stress these stomates partially close, reducing the outflow of water from the plant through transpiration. The stomatal aperture also varies in response to the light intensity. Therefore, in drought conditions and at night, the stomatal resistance would be high, but during the day, with good moisture supply, it would be low. The loss of water through the stomates provides the water potential gradient driving the movement of water and solutes within the plant and in the soil.

The canopy resistance may be evaluated from measurements by rearranging the combination equation to obtain (Bailey and Davies, 1981):

$$r_c = \frac{r_a(SQ_H - \gamma Q_E) + \rho C_p(e_s(T) - e)}{\gamma} \qquad (14)$$

where $e_s(T)$ is the saturation vapour pressure at the reference temperature T. This equation is the one used for the calculation of canopy resistances.

1.5. Objectives

The objectives of this research are as follows:

(1) to measure the components of the energy balance for a suitable field site using two different eddy correlation approaches and to a limited extent, a third profile method;

(2) to compare the latent heat fluxes determined both directly and indirectly from these measurements;

(3) to estimate the canopy resistance of the local crop; and

(4) to evaluate the most likely sources of error in these procedures.

CHAPTER II

THE EXPERIMENT

The purpose of this section is to describe the instrumentation used in this project, along with the appropriate theory and methodology.

2.1. Field Site

The field site was an alfalfa field on a black chernozemic soil at the University of Alberta farm near Ellerslie. The field was relatively flat, uniformly vegetated, possessed a long fetch to the west, and was subject to minimal anthropogenic disturbance. These site requirements are necessary to ensure a horizontally uniform surface layer. The field was chosen mainly for these site requirements and for availability rather than for crop and soil type. A photograph taken by the author of the field site and the general instrumentation appears on Plate 1.

highest anemometer 4.11 m
net radiometer 3.39 m
Lyman-α humidiometer (blue) and sonic anemometer with fine wire thermocouple 2.45 m
psychrometer 2.08 m
middle anemometer 1.64 m
lowest anemometer 0.65 m
soil heat flux plate 5 cm below stake
Bowen ratio equipment on smaller tower to left

Plate 1. Photograph of field site instrumentation looking south.

2.2. Instrumentation

The instrumentation used included an automatically reversing Bowen ratio psychrometer apparatus; a sonic anemometer, a Lyman-α humidiometer, and a fast response thermocouple for eddy correlation measurements; a soil heat flux plate; cup anemometers for determining the wind profile; a net radiometer; and the requisite ancillary equipment and data logging capability. The equipment will be described piece-by-piece with emphasis being placed on the Bowen Ratio device, unique to this experiment, and then the combined operation and data collection will be explained.

2.3. Bowen Ratio Device

The Bowen ratio defined earlier is given by Eq. (1). If we assume horizontal uniformity, then Q_H and Q_E are constant with height and by the Ohm's law analogy, we can relate the fluxes to differences in temperature and vapour pressure across a finite height interval Δz, viz:

$$Q_H = \rho C_p \overline{\Delta T} \, r_H^{-1} \tag{15}$$

and

$$Q_E = \rho C_p \, (\overline{\Delta e} \, \gamma^{-1}) \, r_v^{-1} \tag{16}$$

where γ, the psychrometric constant, is determined from:

$$\gamma = \frac{pC_p}{0.622\ L} \tag{17}$$

Therefore,

$$B = \frac{Q_H}{Q_E} = \frac{\rho C_p\ \overline{\Delta T}\ r_H^{-1}}{C_p(\overline{\Delta e}\ \gamma^{-1})\, r_v^{-1}} = \frac{\overline{\Delta T}}{\overline{\Delta e}\ \gamma^{-1}} \tag{18}$$

where r_H has been found empirically to be closely equal to r_v.

The change in wet and dry bulb temperatures between two levels in the atmosphere can be measured by matched psychrometers at those two levels. The difference in vapour pressure is then found as follows.

The vapour pressure is related to the wet and dry bulb temperatures by:

$$e = e_s(T_w) - \gamma(T - T_w) \tag{19}$$

Therefore, using an approximation which gets better for smaller ΔT_w:

$$\begin{aligned} \Delta e &= e_s(T_{w2}) - e_s(T_{w1}) - \gamma(T_2 - T_1 - (T_{w2} - T_{w1})) \\ &\cong S(T_{w2} - T_{w1}) - \gamma(T_2 - T_1) + \gamma(T_{w2} - T_{w1}) \\ &= (S + \gamma)\ \Delta T_w - \gamma \Delta\ T \end{aligned} \tag{20}$$

where S, the slope of the saturation vapour pressure curve, is defined by:

$$S(T_w) = \frac{Le_s}{R_v T_w^2} \qquad (21)$$

where R_v is the gas constant for water vapour. The Bowen ratio, then, can be calculated from the difference between two levels in the wet and dry bulb tempeatures. Such a device is theoretically simple but requires considerable effort to give satisfactory results. The standard practise is to set up the psychrometers on a device that will reverse their position on a regular interval in order to reduce systematic error arising from differences in response between imperfectly matched psychrometers. The psychrometers must be well shielded and ventilated in order to avoid errors due to radiational heating and the wet bulb thermometer wicks must be kept constantly wet with distilled water. An additional complication arises because the temperature values are useful and worth storing only after a sufficient wait for temperature stabilization has occurred after each reversal.

The device developed for this project is pictured in Plate 2. The main structure of the device was made of a 2 m length of PVC pipe with a 3/4" inner (≅1.91 cm) and a 1" outer (≅2.54 cm) diameter. The psychrometers extended upwind at right angles at each end of the length

Plate 2. Frontal view of reversing psychrometer apparatus as used in 1988 field season. View is to the east. (Photograph taken by author.)

and the reversing motor and mounting to the tower were at the middle.

The diameter of the pipe was minimized to reduce the stress on the reversing motor and to increase the ventilation speed across the psychrometers. A sketch of the main reversing arm assembly is shown on Figure 1. The psychrometers were constructed using 8 inches of 40-gauge chromel-constantin thermocouple wire joined to stronger 24-gauge thermocouple wire to make the connection with the data logger. Calculations indicated that, with 40-gauge wire, conduction to the thermocouple junction would not cause significant error.

The sensor heads were constructed by inserting a junction of the 40-gauge thermocouple wire into a shrink tube molding attached to a 1 1/4 inch Polyethylene T. The junction was potted with 5-minute epoxy. The time constant for the thermocouple junctions was measured to be about 30 seconds. A sketch giving details of the psychrometers is shown on Figure 2. The junction between the 40-gauge and the 24-gauge wire and temperature sensors themselves was delicate, so care was taken to minimize tension along the connecting wires by clamping them down.

The device was ventilated by a fan connected by a hose to the top of the T fitting at the middle of the arm. The fan was a PAPST Type RL 90-18/12 12-Volt DC centrifugal fan rated at 40 cubic metres per hour. The

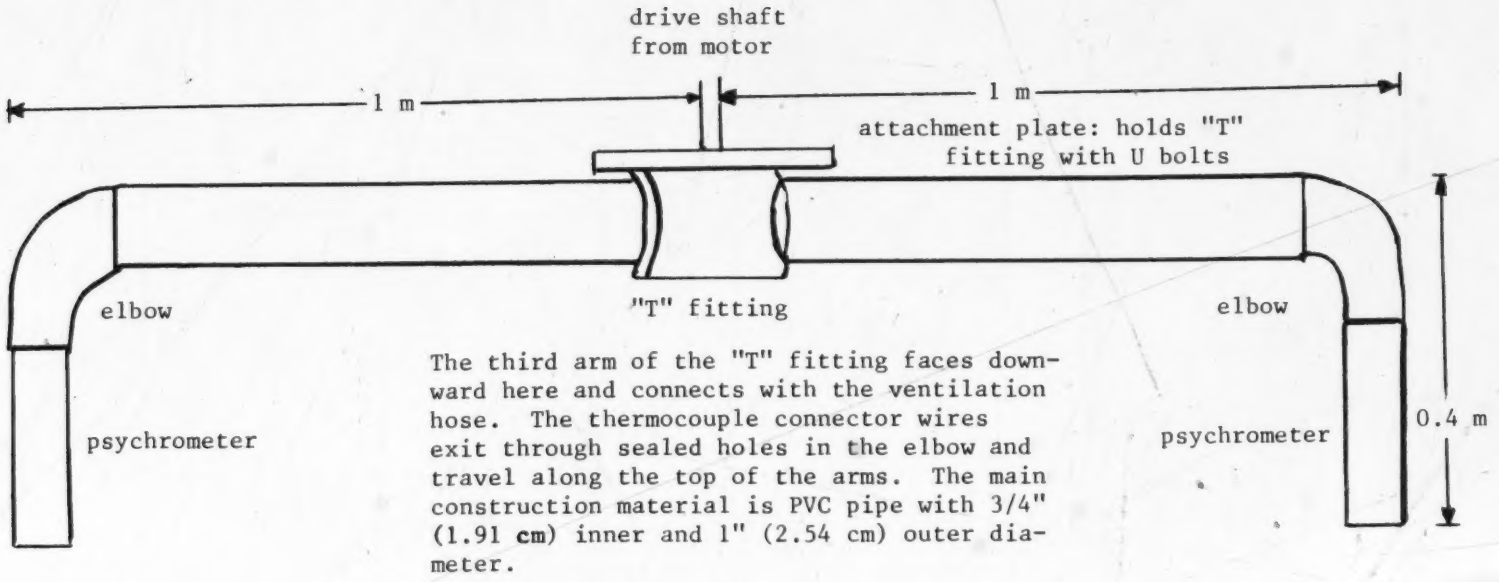
drive shaft
from motor
1 m
1 m
attachment plate: holds "T"
fitting with U bolts
elbow
"T" fitting
elbow
psychrometer
psychrometer
0.4 m
The third arm of the "T" fitting faces downward here and connects with the ventilation hose. The thermocouple connector wires exit through sealed holes in the elbow and travel along the top of the arms. The main construction material is PVC pipe with 3/4" (1.91 cm) inner and 1" (2.54 cm) outer diameter.

Figure 1. Top view sketch of reversing psychrometer arm.

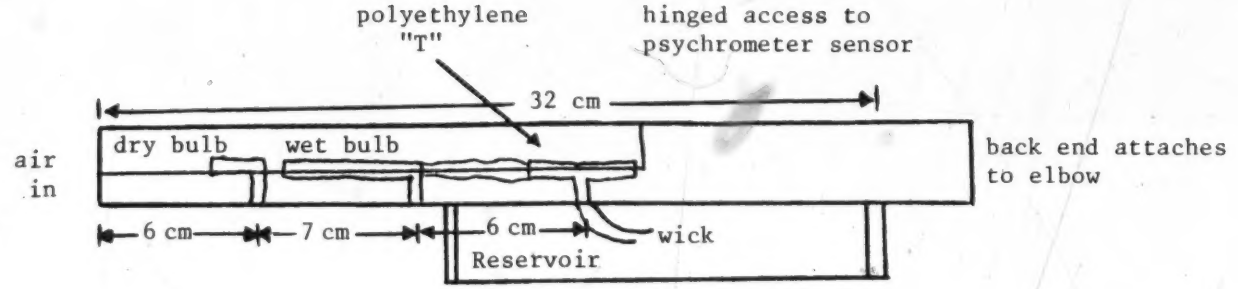

Vertical diameter of both parts: 1" (2.54 cm) outer, 3/4" (1.91 cm) inner

Lower tube: water reservoir, back end cemented.
Front end removable for refilling, which is routed
from wet bulb sensor through "T" into the reservoir.
In the field this was covered by form fitting foam
wrapped in 3M reflective tape.

Figure 2. Sketch of psychrometers: side view.

flow rate across the psychrometer junction was difficult to measure exactly but exceeded 5 m/s.

The shielding for the psychrometers consisted of form-fitting foam covered with 3M reflective tape.

The motor used to reverse the arm was a TRW EM-15/409A6054-2 12-Volt DC planetary gear motor rated at a maximum continuous torque of 1250 ounce-inches. The details of how this was mounted are shown on Figure 3. Both this motor and the fan were powered by standard 12V automotive batteries.

The printed circuit board that controlled the reversing of the device allowed both manual (push button) and automatic reversal through programmed excitation pulses sent by the data logger (Figure 4).

The instrument was mounted on the tower such that the lower psychrometer was 0.97 metres above the ground and the upper psychrometer was 2.20 metres above the ground. The two psychrometers were found to be very closely matched when tested in the laboratory. Despite this close matching it is still necessary to reverse, to reduce radiation error.

2.4. Sonic Anemometer

The sonic anemometer used for this research was a Campbell Scientific CA27 and it was used to obtain fluctuations in the vertical windspeed, which are

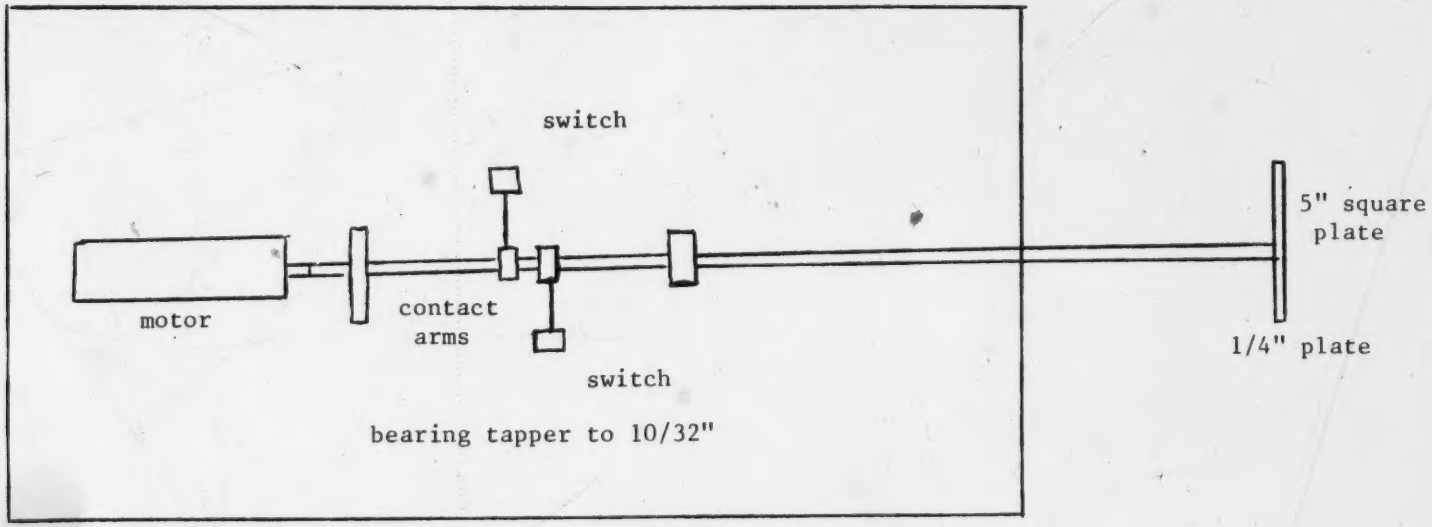

Scale: 1" = 4"

The switches send a pulse to stop the motor when full travel is completed in a reversal.

Figure 3. Details of motor mount.

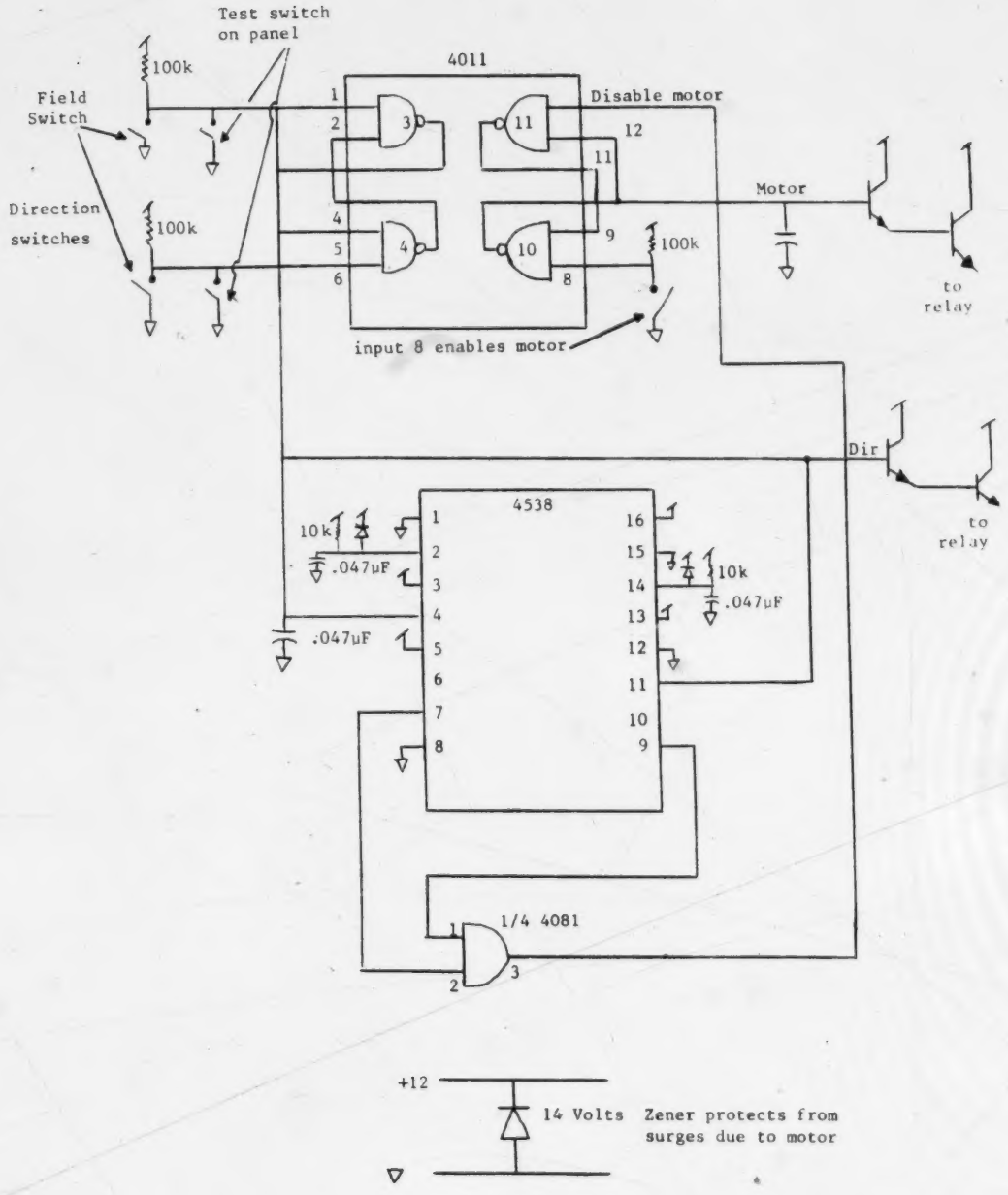

Figure 4. Sketch of Bowen ratio device motor control circuit.

generally of the order of 1 m/s. The calibration response of a CA27 is one volt per metre per second with a range between plus and minus four volts. This device was mounted on the tower at a height of 2.45 metres.

2.5. Fine Wire Thermocouple

The fine wire thermocouple is mounted on the arm with the sonic anemometer on the CA27. It is a 5.0×10^{-4} inch (1.96×10^{-6} m) diameter chromel constantan thermocouple. The calibration on the thermocouple is 0.25 Volts per degree Celsius within a range of plus or minus 4 Volts. The temperature signal received is the fluctuation relative to the temperature within the sonic anemometer case which has a much higher thermal inertia. This was mounted to the tower at a height of 2.45 metres.

2.6. Net Radiometer

The net radiation was measured using a Q*4 net radiometer manufactured by Radiation Energy Balance Systems (REBS) of Seattle, Washington. The instrument was new at the time of this research and was factory calibrated at 10.1 W m^{-2} mV^{-1}. The net radiometer was mounted on the tower at a height of 3.39 metres.

2.7. Heat Flux Plate

The soil heat flux was measured using a soil heat flux plate manufactured and calibrated in the meteorology lab at the University of Alberta. The calibration factor was 4 W m^{-2} mV^{-1}. This was buried under 5 cm of soil in a relatively undisturbed site near the instrument tower. No correction for heat storage in the soil layer above the flux plate was attempted. An estimate of the error associated with this measurement is in Section 3.4.

2.8. Lyman-α Humidiometer

The Lyman-α Humidiometer was manufactured by the Electromagnetic Research Corporation of College Park, Maryland. It was mounted on the tower at a height of 2.45 metres and was used to detect rapid fluctuations in the water vapour concentration. At the Lyman-α frequency the absorption coefficient of water vapour far exceeds that of other gases in the lower atmosphere so that the amount of Lyman-α radiation transmitted through the atmosphere is inversely proportional to the concentration of water vapour in that air. The output current of the Lyman-α humidiometer has been found to obey:

$$I = I_o e^{-\mu \rho_v d} \qquad (22)$$

where I_o depends upon the source tube condition and detector sensitivity, d is the length of the measuring path, μ is the absorption coefficient of water vapour, and ρ_v is the absolute humidity of the air in the path-length.

This device was calibrated in the meteorology lab against an EG+G dewpoint hygrometer. The calibration curves are shown on Figure 5. Note that the curves are essentially linear.

2.9. Ancillary Equipment

A gasoline-powered electrical generator was used to power the Lyman-α and the fan that provided aspiration to the psychrometer mounted on the tower.

A psychrometer, made and calibrated in the University of Alberta meteorology lab, was mounted on the tower at the 2.08 metre level. This was needed to measure absolute wet and dry bulb temperatures since the Bowen ratio equipment was set up to measure differential temperatures between two levels. The absolute temperatures were necessary to calculate the canopy resistances.

Cup anemometers were set at heights of 0.65 m, 1.64 m, and 4.11 m on the tower in order to provide the data necessary to infer the aerodynamic resistance. From knowledge of the wind profile based on the wind speeds at

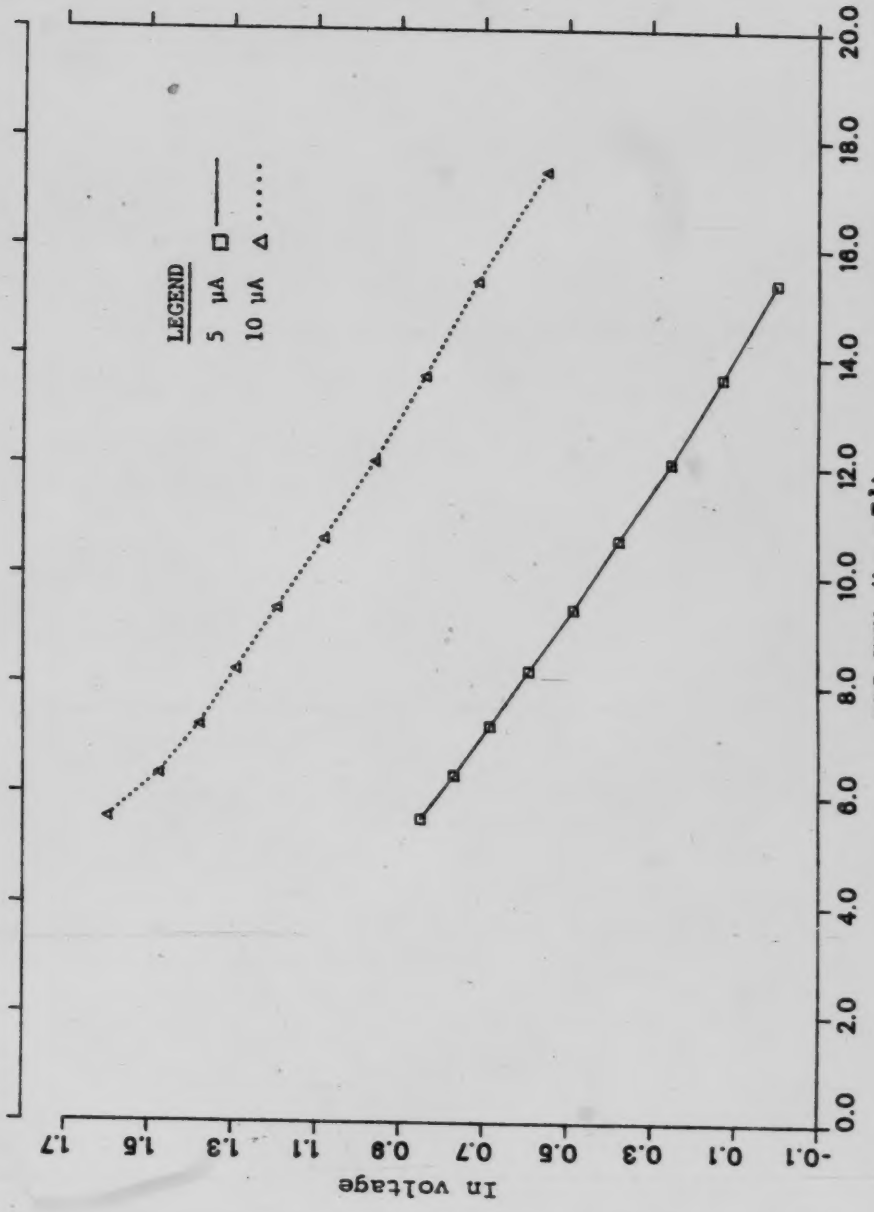

Figure 5. Calibration curves for Lyman-α humidiometer.

these three levels, it was possible to deduce wind speeds at intermediate levels using a least squares curve fit.

The data logger used in this research was a Campbell Scientific CR21X. The signals from all instruments, except for the Bowen ratio device, were connected to this logger and were accessible in real time as well as being averaged and stored in output locations in the logger's memory. The Bowen ratio device was separately connected to a Campbell Scientific CR-7 logger. The main program used in the CR21X for this field study with notes on the assigned input and output locations is given in Appendix 1.

CHAPTER III

FIELD RESULTS

This section will present an overview of the data obtained from the instruments during this research. This will be largely shown in a graphical format. The data manipulation necessary to obtain these graphical representations will also be discussed.

3.1. Energy Balances

The energy balances as measured by the instrumentation used in this study are shown in figures 6 through 16. On these figures $Q^* - Q_G$ is derived directly by subtracting the soil heat flux from the net radiative flux as output in the CR21X. The CR21X was programmed to output these values in their proper units for simplicity and ease of inspection. The Q_H value is obtained through calculations using the CR21X output locations for $\overline{w}$, $\overline{T}$, and $\overline{wT}$, and by using,

$$Q_H = \rho C_p \overline{w'T'} = \rho C_p (\overline{wT} - \overline{w}\,\overline{T}) \qquad (23)$$

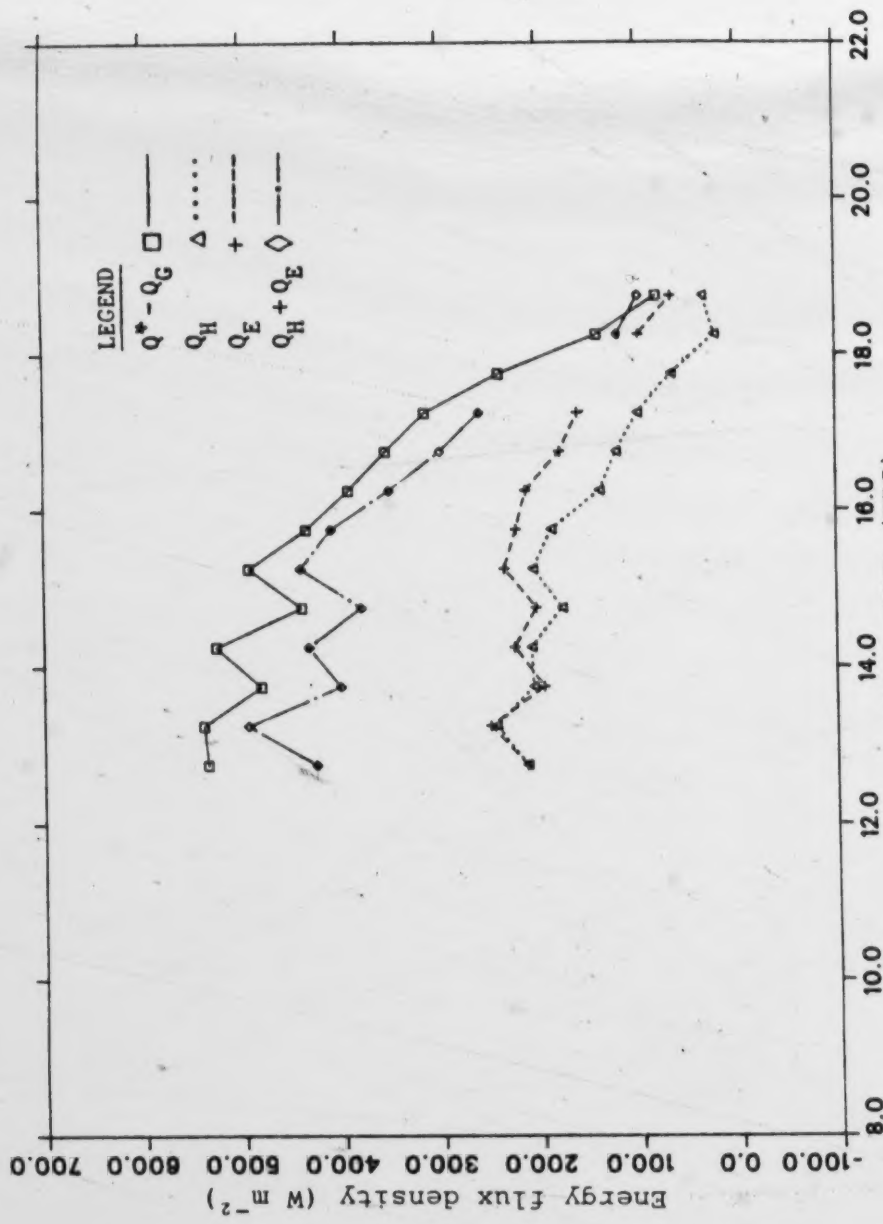

Figure 6. Components of the energy balance for May 15, 1988.

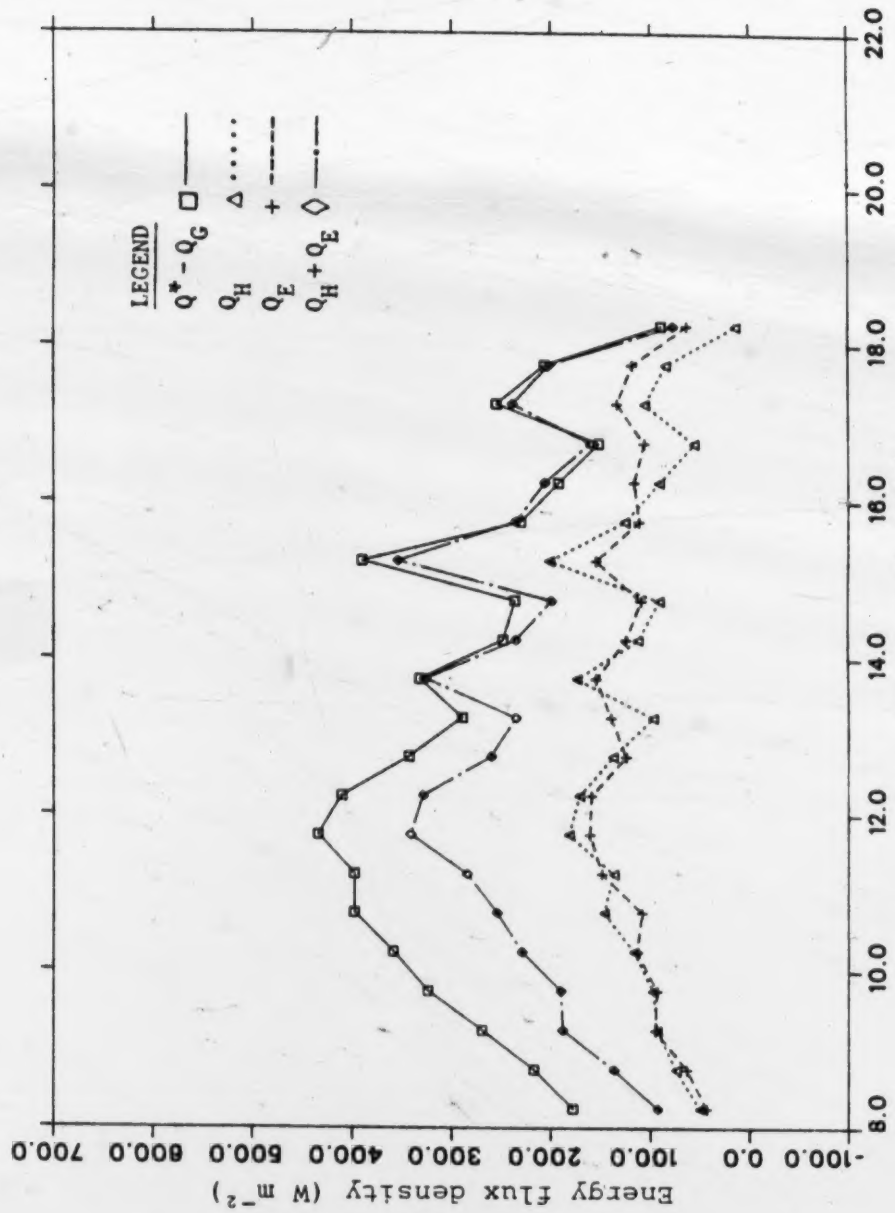

Figure 7. Components of the energy balance for May 16, 1988.

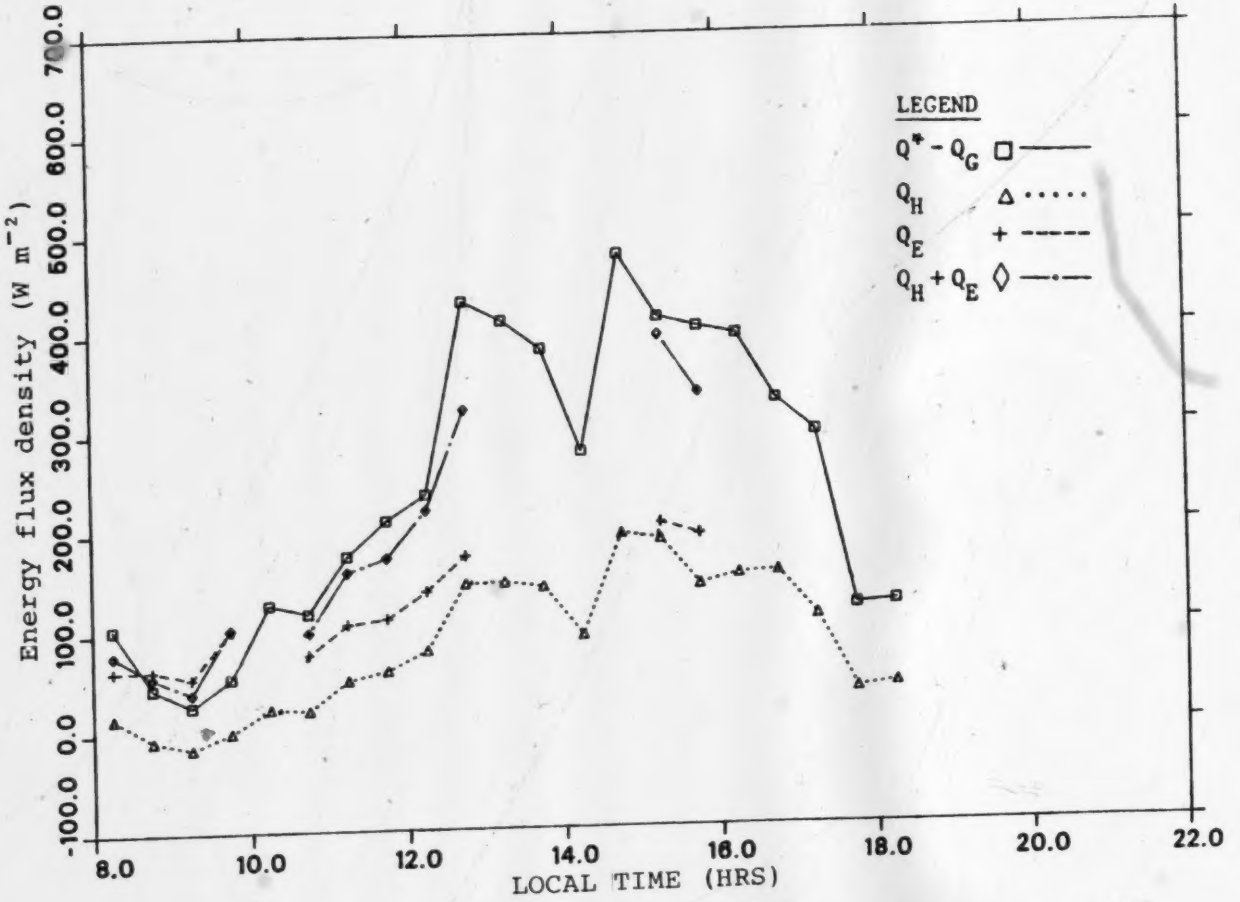

Figure 8. Components of the energy balance for May 17, 1988.

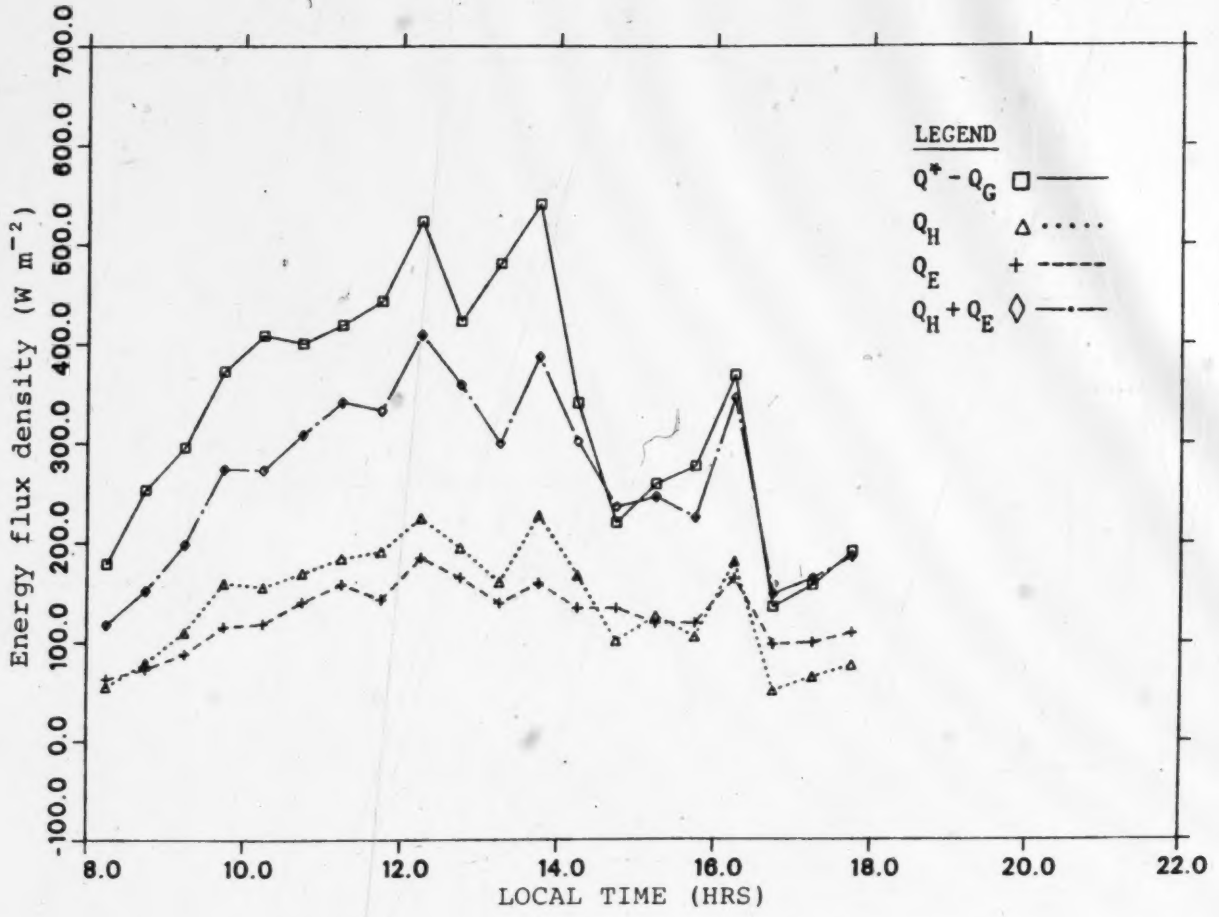

Figure 9. Components of the energy balance for May 18, 1988.

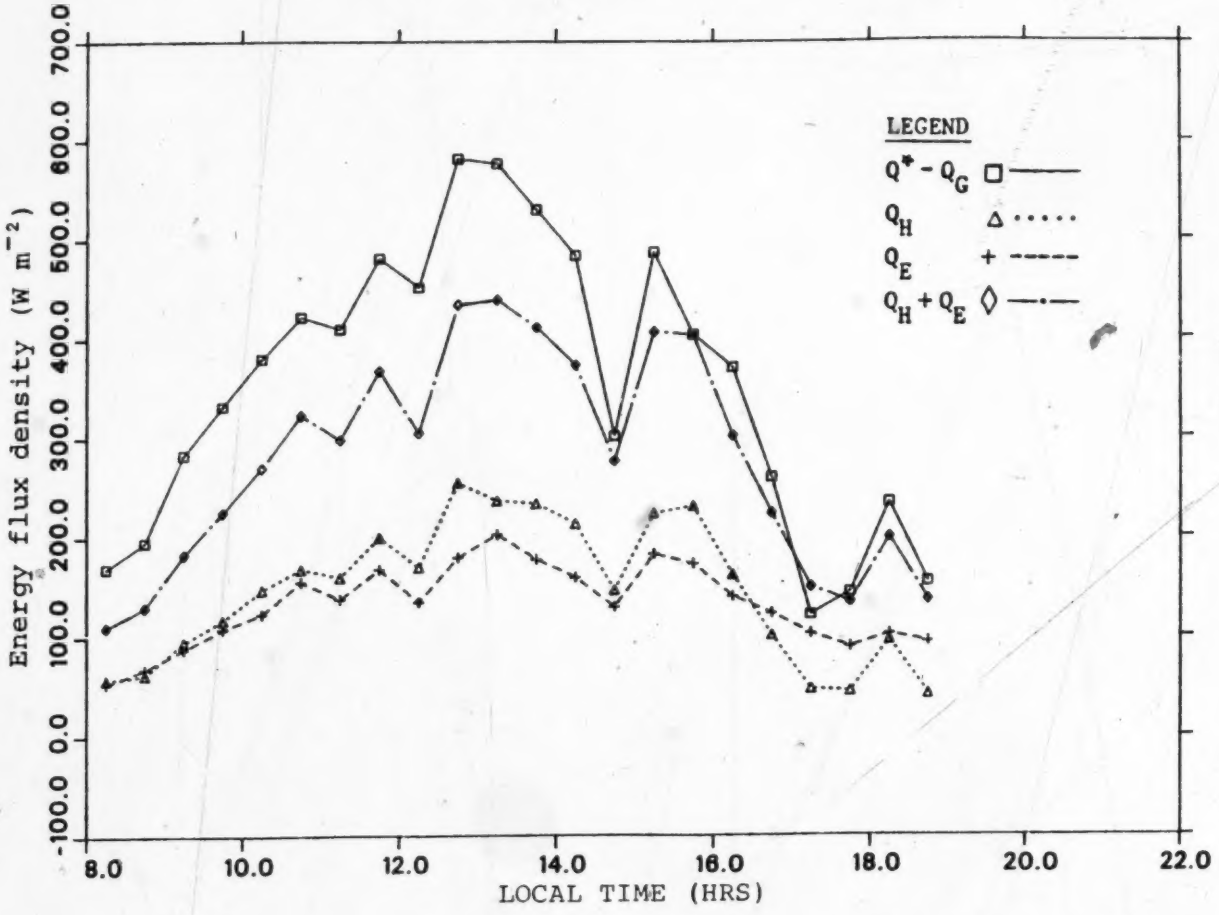

Figure 10. Components of the energy balance for May 19, 1988.

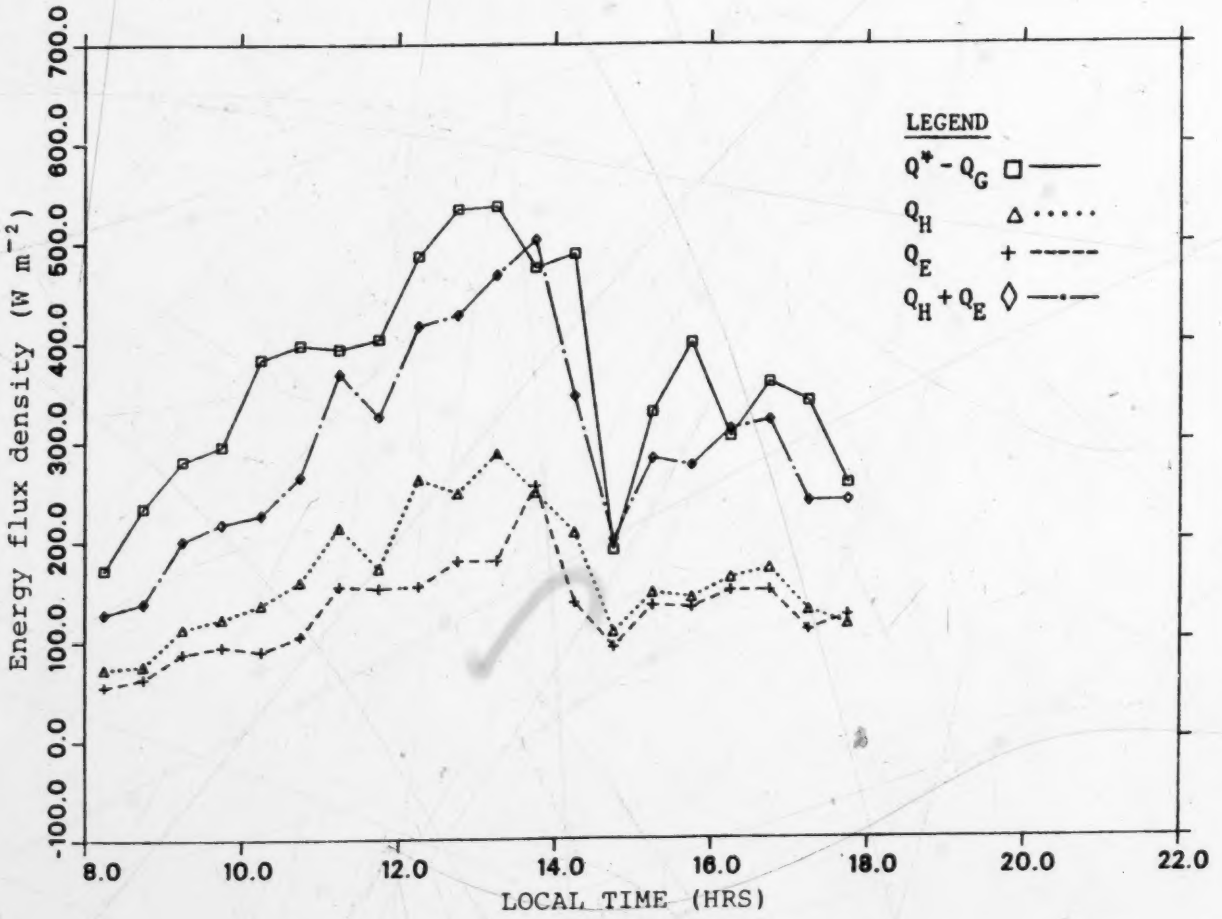

Figure 11. Components of the energy balance for May 20, 1988.

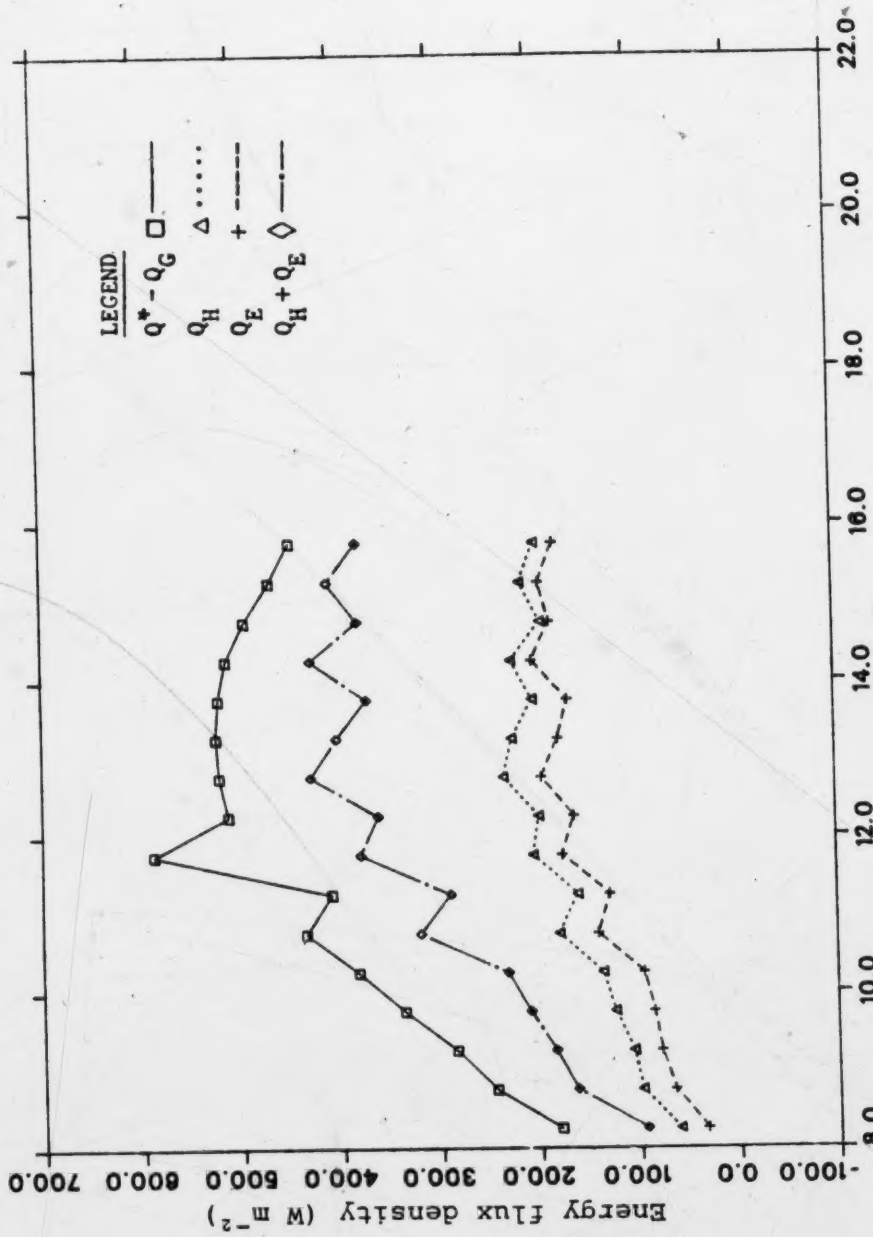

Figure 12. Components of the energy balance for May 21, 1988.

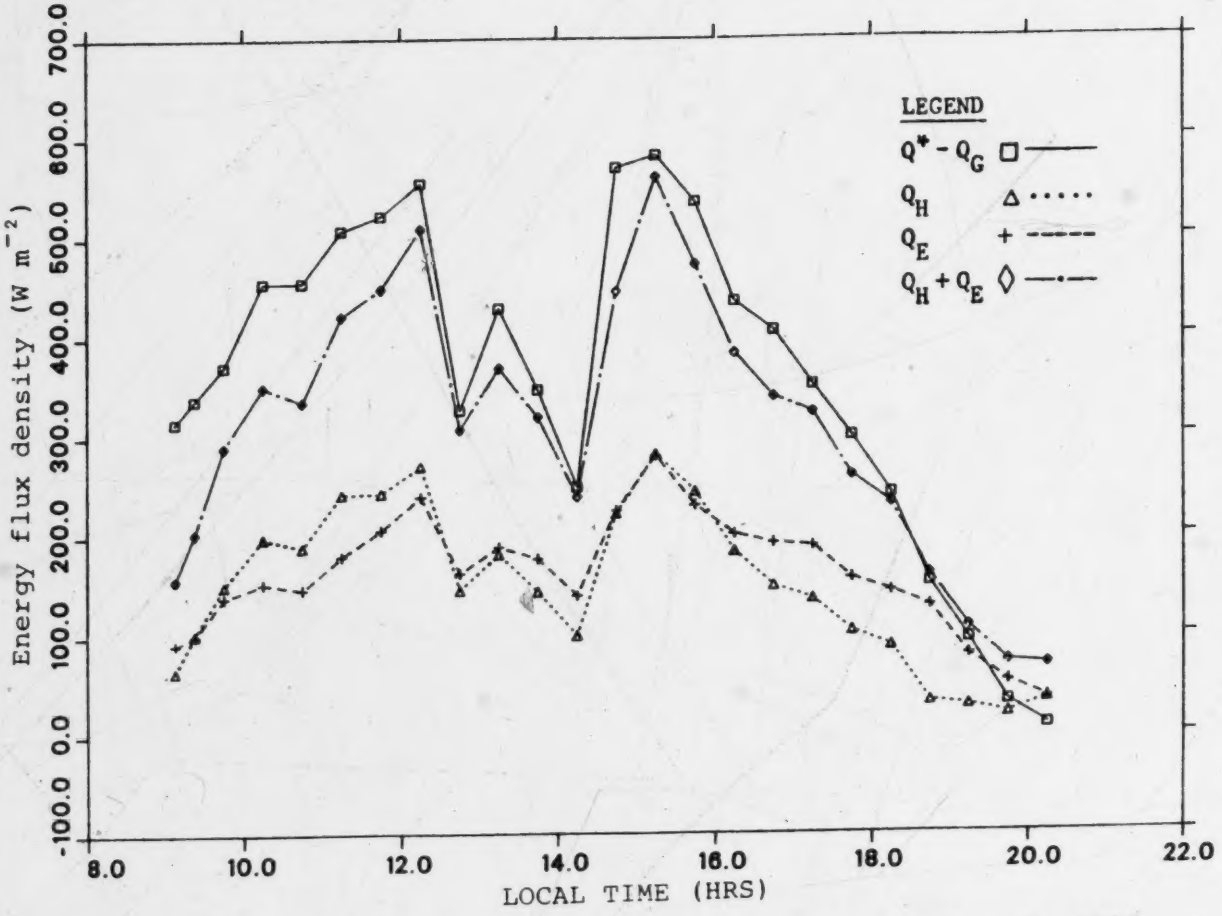

Figure 13. Components of the energy balance for June 2, 1988.

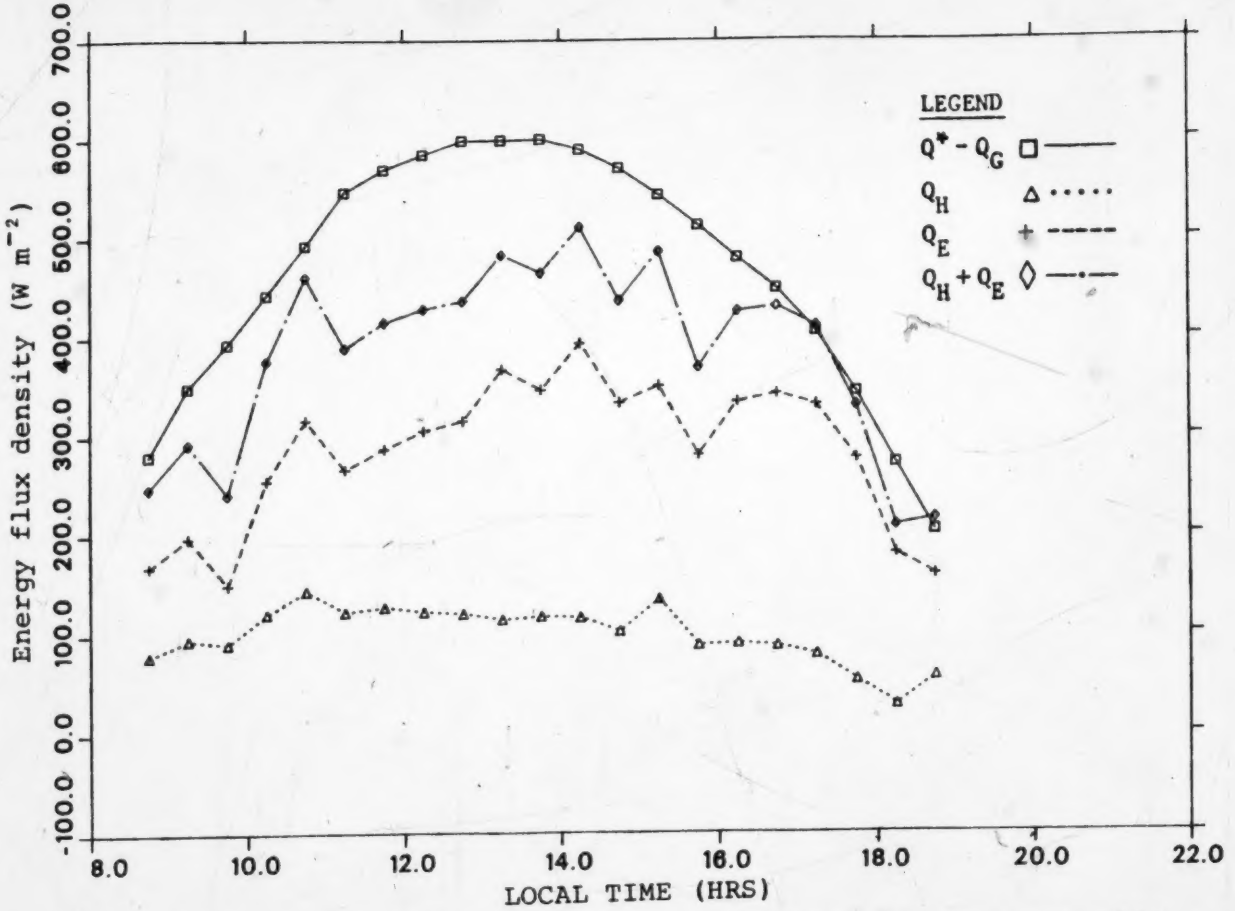

Figure 14. Components of the energy balance for June 14, 1988.

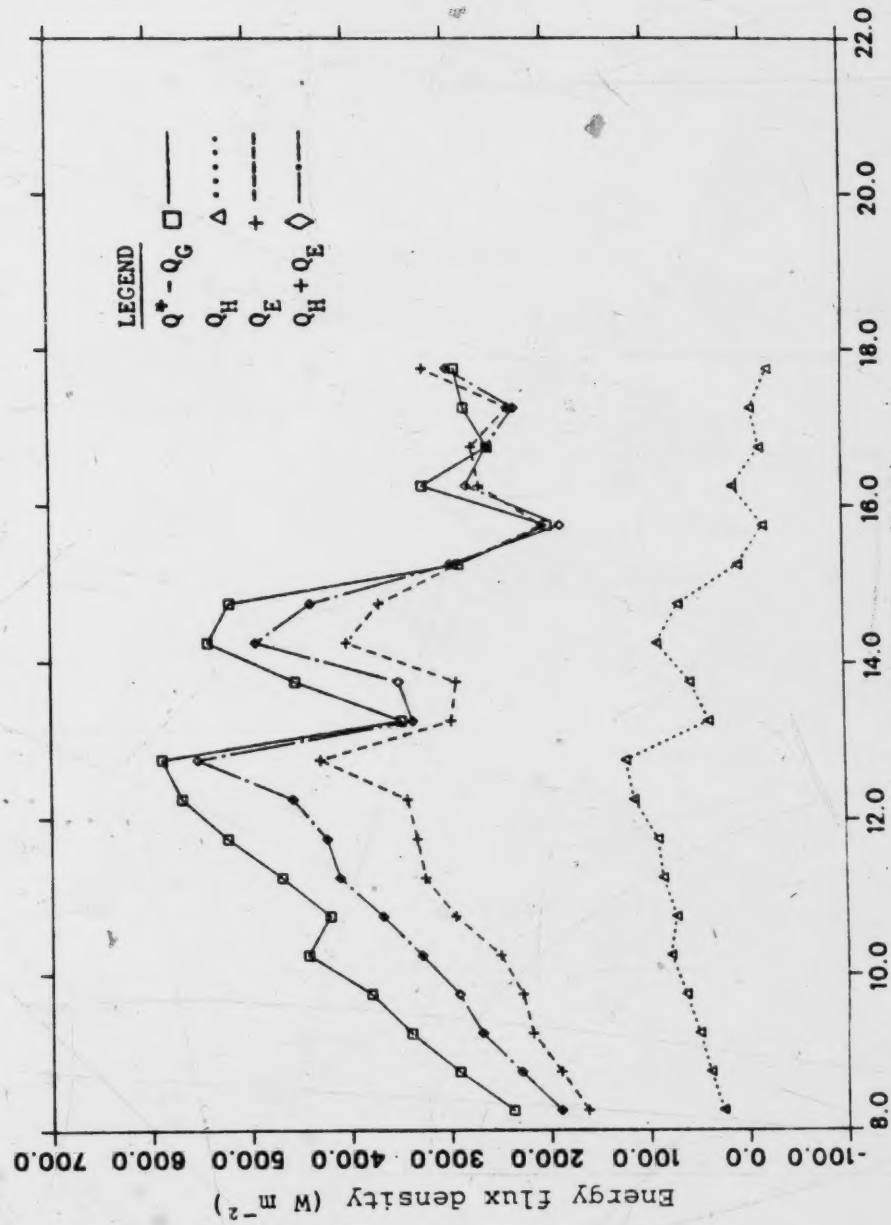

Figure 15. Components of the energy balance for June 15, 1988.

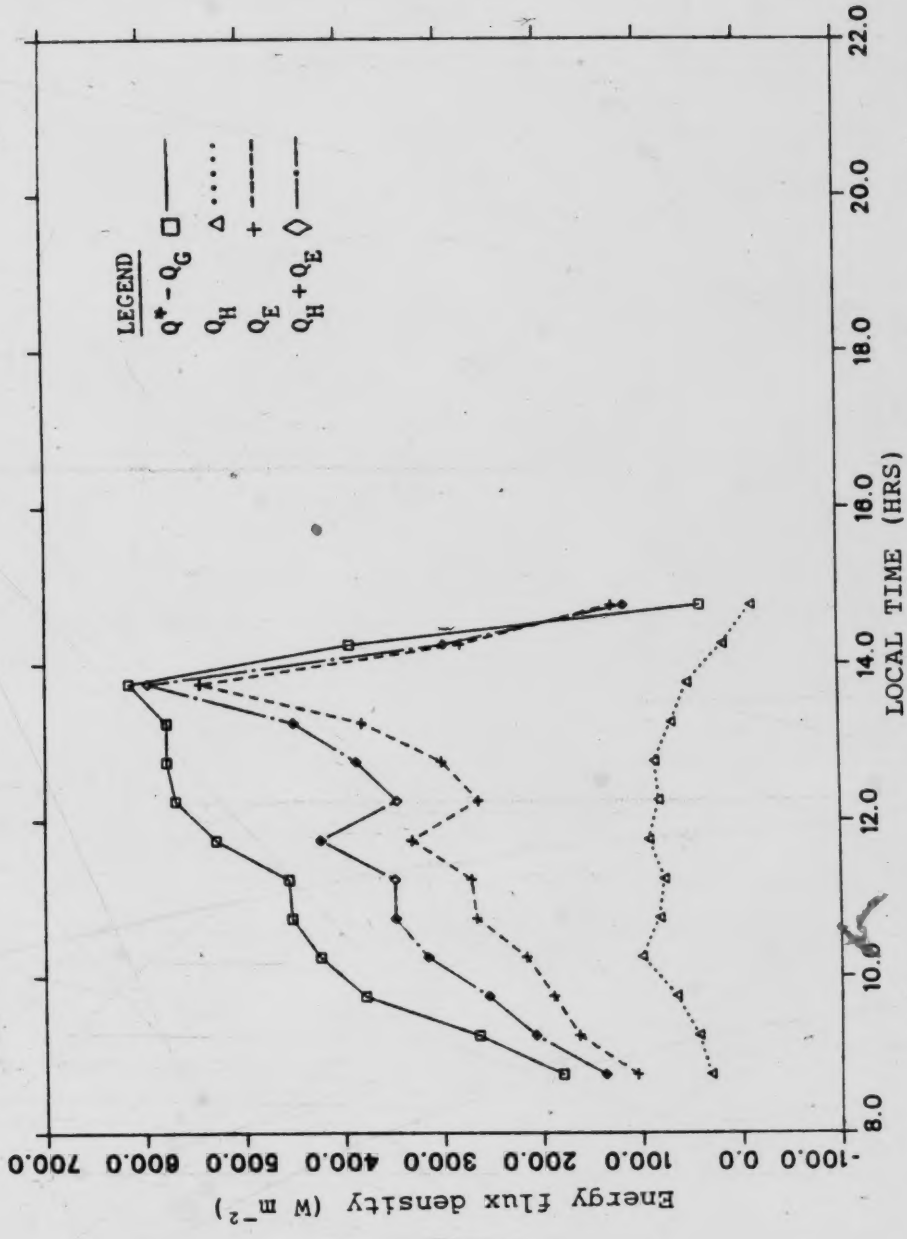

Figure 16. Components of the energy balance for June 23, 1988.

as discussed in Chapter I. The density was calculated from the Edmonton station pressure and mean temperature. The Q_E value was similarly found from the CR21X output locations for $\bar{w}$, ρ_v, and $\overline{w\rho_v}$ and by using,

$$Q_E = L\,\overline{w'\rho_v'} = L(\overline{w\rho_v} - \bar{w}\,\bar{\rho}_v) \qquad (24)$$

The sum of Q_E and Q_H should equal Q^* minus Q_G; however, it is notable from the figures that this was often not the case, especially in the morning. Another point of interest in these energy balances is the way in which the availability of moisture affected the Bowen ratio with drier days clearly showing the higher values (see Table 1). It is also interesting to see how dramatically the available energy $Q^* - Q_G$ dropped off in Figure 16 as a large thunderstorm approached around 1400 local time.

3.2. Comparative Latent Heat Fluxes

Figures 17 to 26 show the latent heat fluxes as measured by the field instrumentation. The following symbols will be defined to indicate the method by which the flux was calculated:

$$Q_E^{(w-r_v)} = L(\overline{w\rho_v} - \bar{w}\,\bar{\rho}_v) \qquad (25)$$

$$Q_E^{-(w-t)} = Q^* - Q_G - \rho C_p(\overline{wT} - \bar{w}\,\bar{T}) \qquad (26)$$

Table 1. Summary of total rainfall (R_t), daily average Bowen ratios (BR), mid-day canopy resistances (r_c), and temperatures ($\overline{T}$).

Date	R_t (mm)	BR	r_c	$\overline{T}$
May 1-12	0.0			
13	1.0			
14	6.0			
15	0.0	0.77	96.5	10.0
16	0.0	0.88	264.1	17.2
17	tr	0.49	108.8	11.9
18	0.0	1.07	177.4	12.0
19	0.0	1.06	257.6	10.2
20	0.0	1.28	153.6	11.8
21	0.0	1.28	279.7	12.9
30	9.0			
June 1	0.4			
2	0.0	0.88	97.1	13.3
5	11.0			
7	0.4			
8	39.6			
9	5.0			
10	0.2			
11	10.4			
13	3.4			
14	0.0	0.36		12.6
15	1.6	0.13		17.5
18	3.8			
22	10.2			
23	4.0	0.23		17.7

Note: No rainfall occurred, and no field measurements were taken on May 22-29, May 31, June 3-4, June 6, and June 16-17. No canopy resistances were calculated for June 14, 15 and 23.

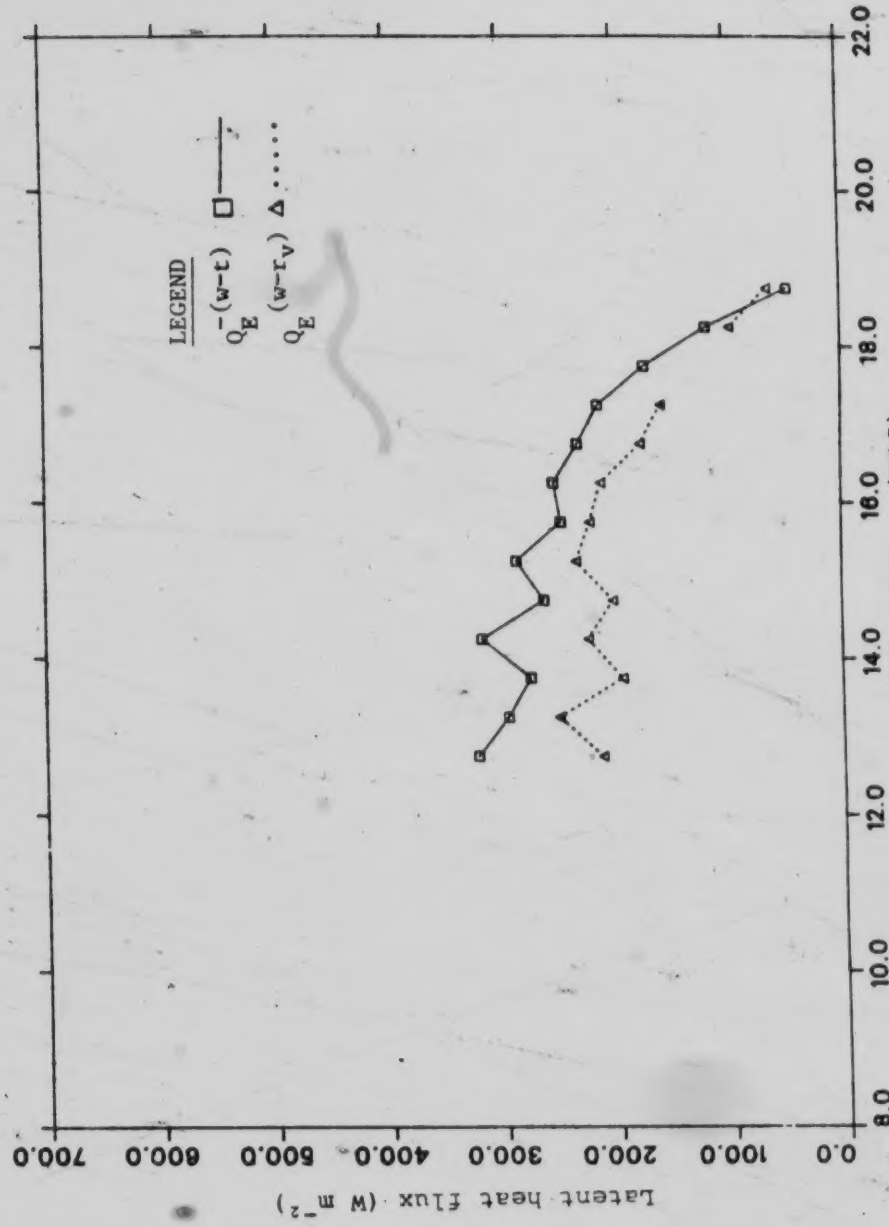

Figure 17. Comparative latent heat fluxes for May 15, 1988.

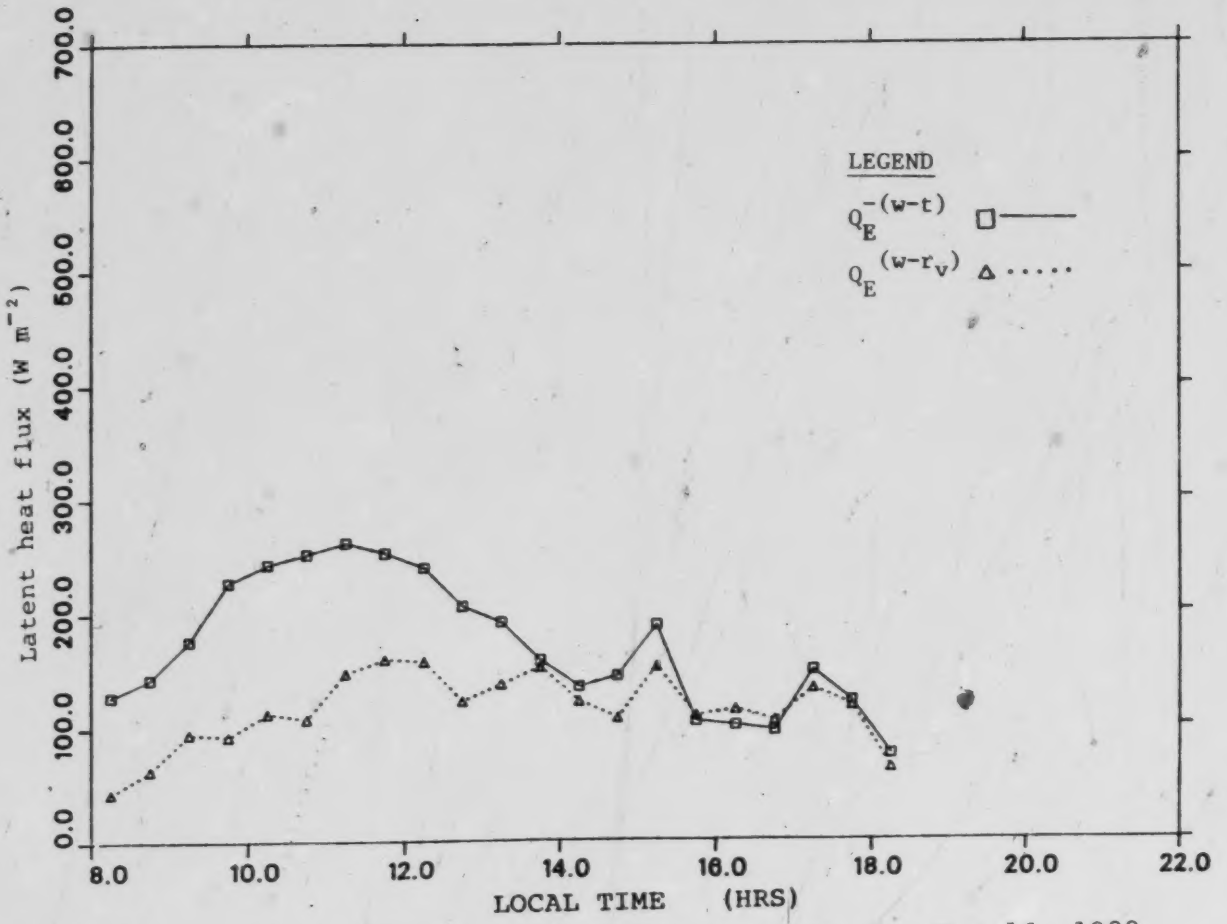

Figure 18. Comparative latent heat fluxes for May 16, 1988.

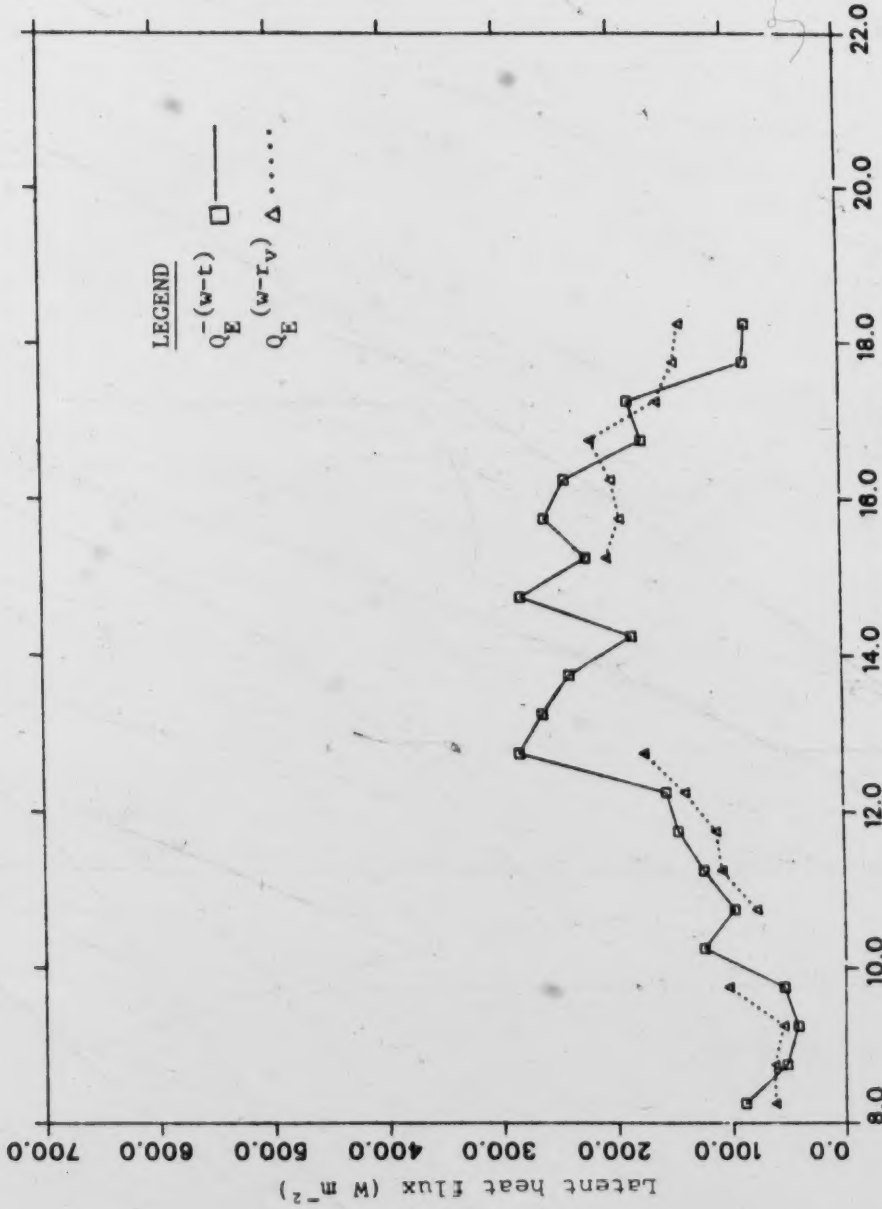

Figure 19. Comparative latent heat fluxes for May 17, 1988.

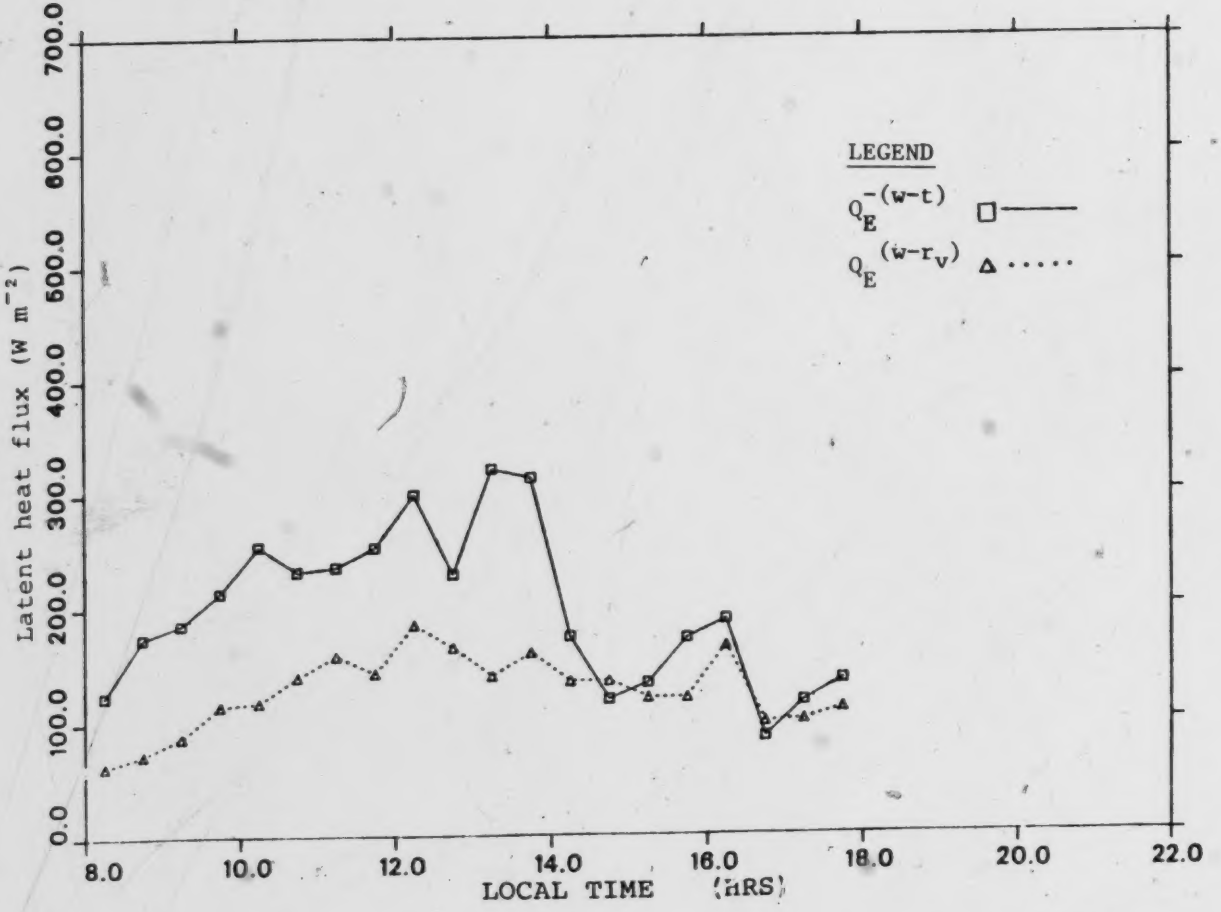

Figure 20. Comparative latent heat fluxes for May 18, 1988.

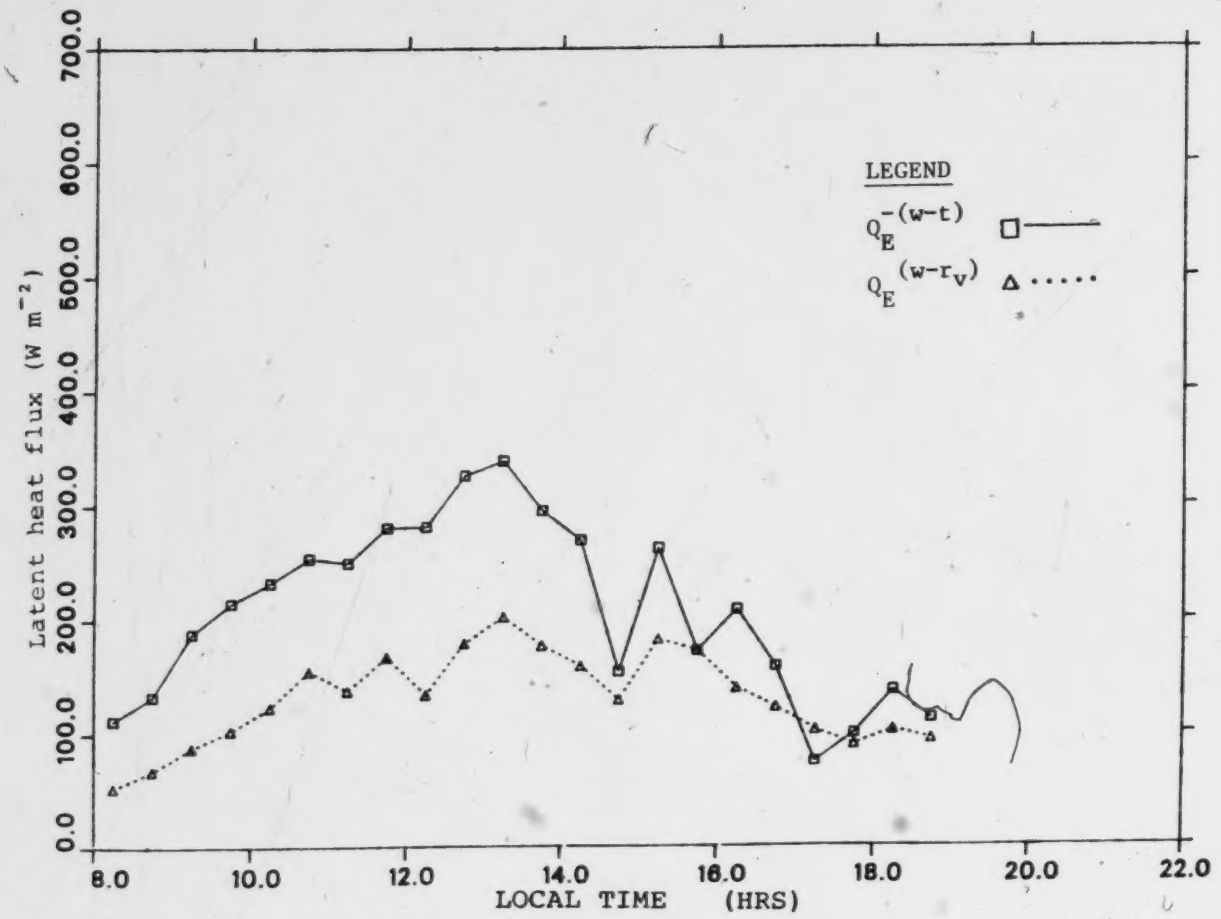

Figure 21. Comparative latent heat fluxes for May 19, 1988.

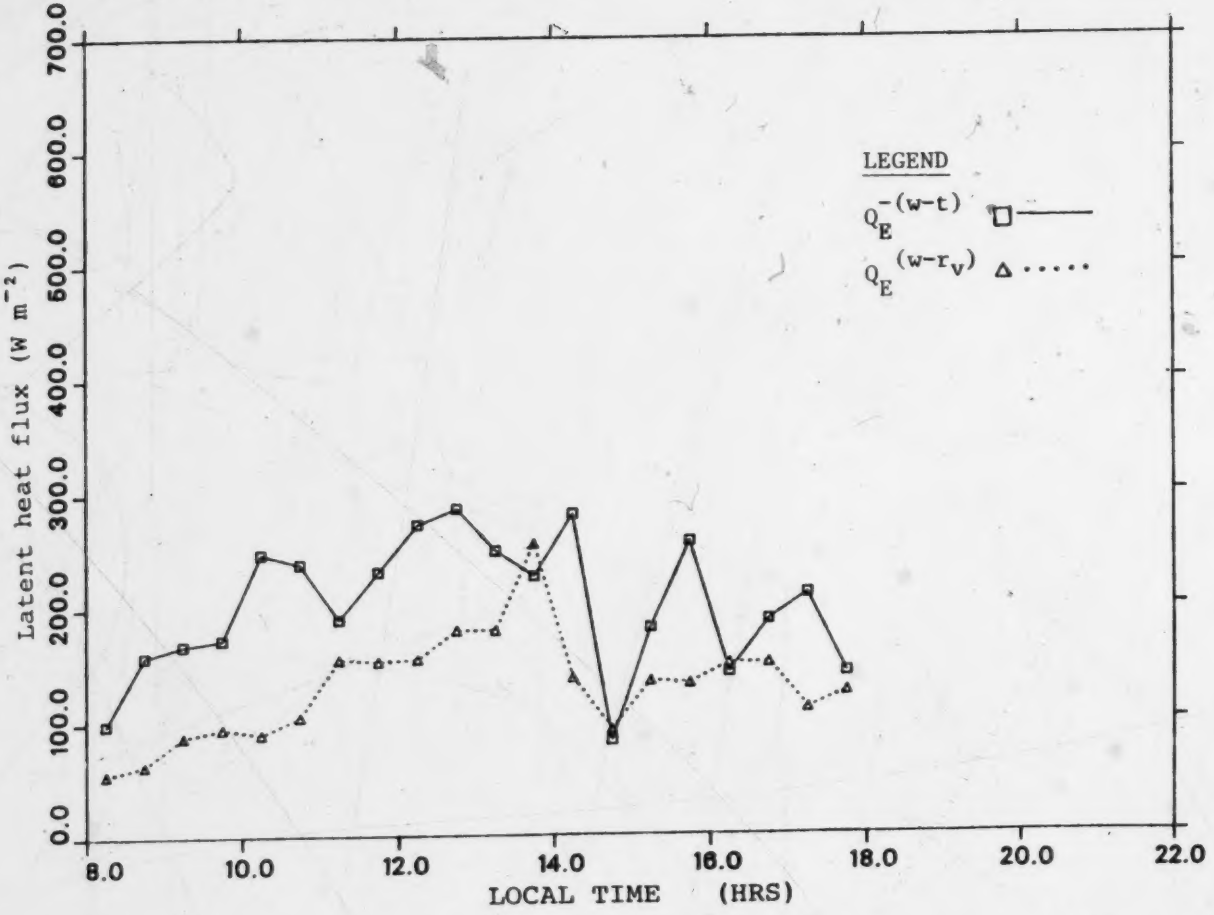

Figure 22. Comparative latent heat fluxes for May 20, 1988.

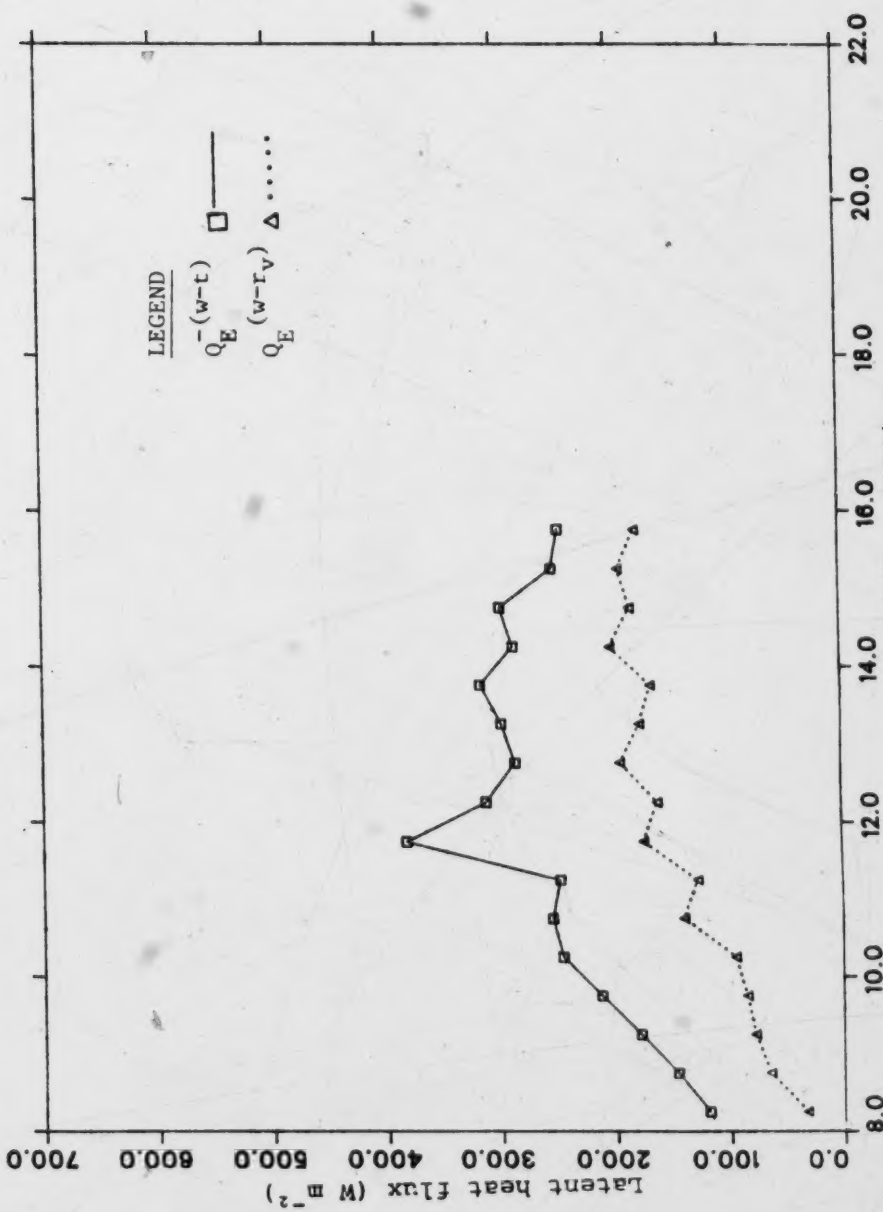

Figure 23. Comparative latent heat fluxes for May 21, 1988.

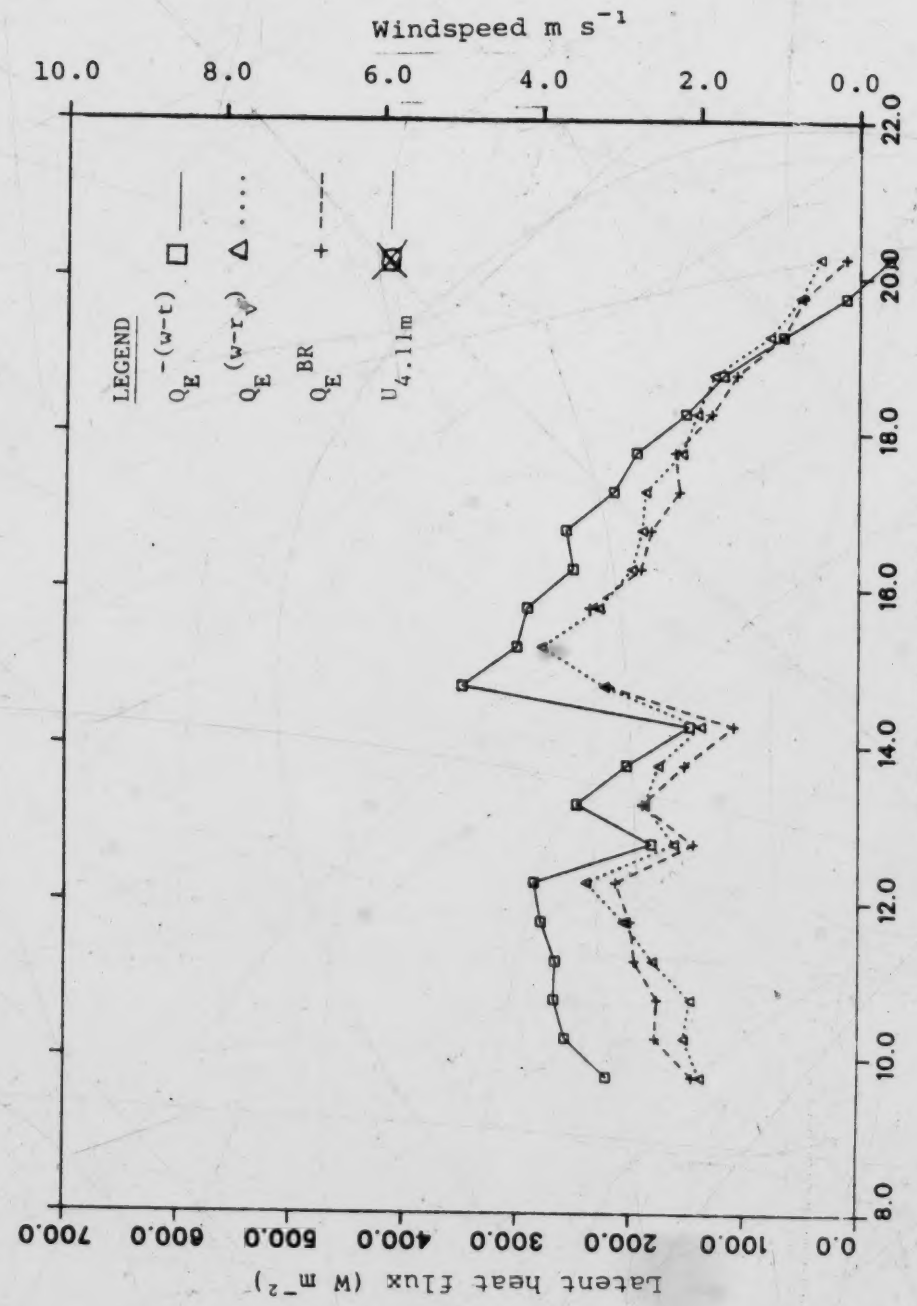

Figure 24. Comparative latent heat flux for June 2, 1988 with coplotted 4.11 m windspeed.

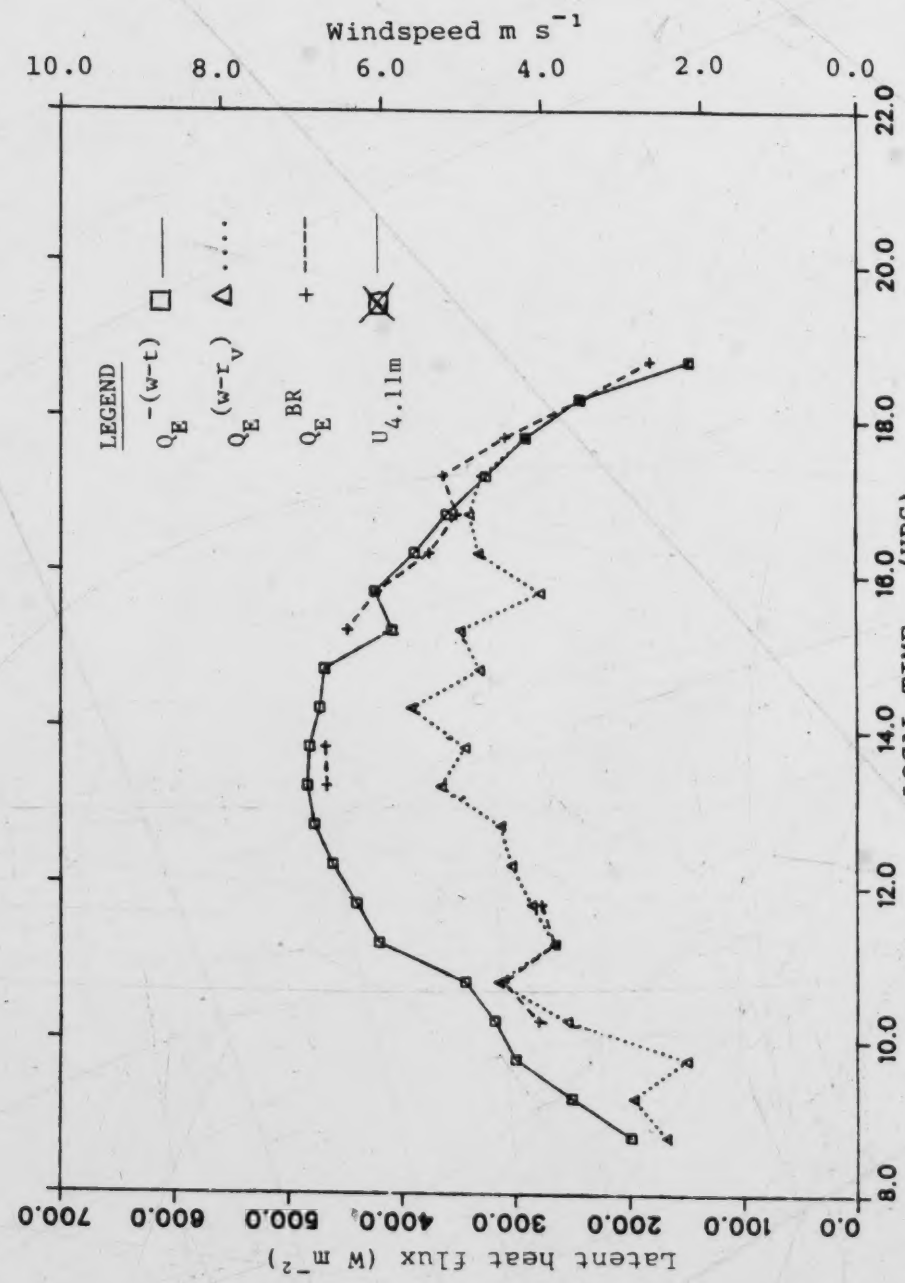

Figure 25. Comparative latent heat flux for June 14, 1988 with coplotted 4.11 m windspeed.

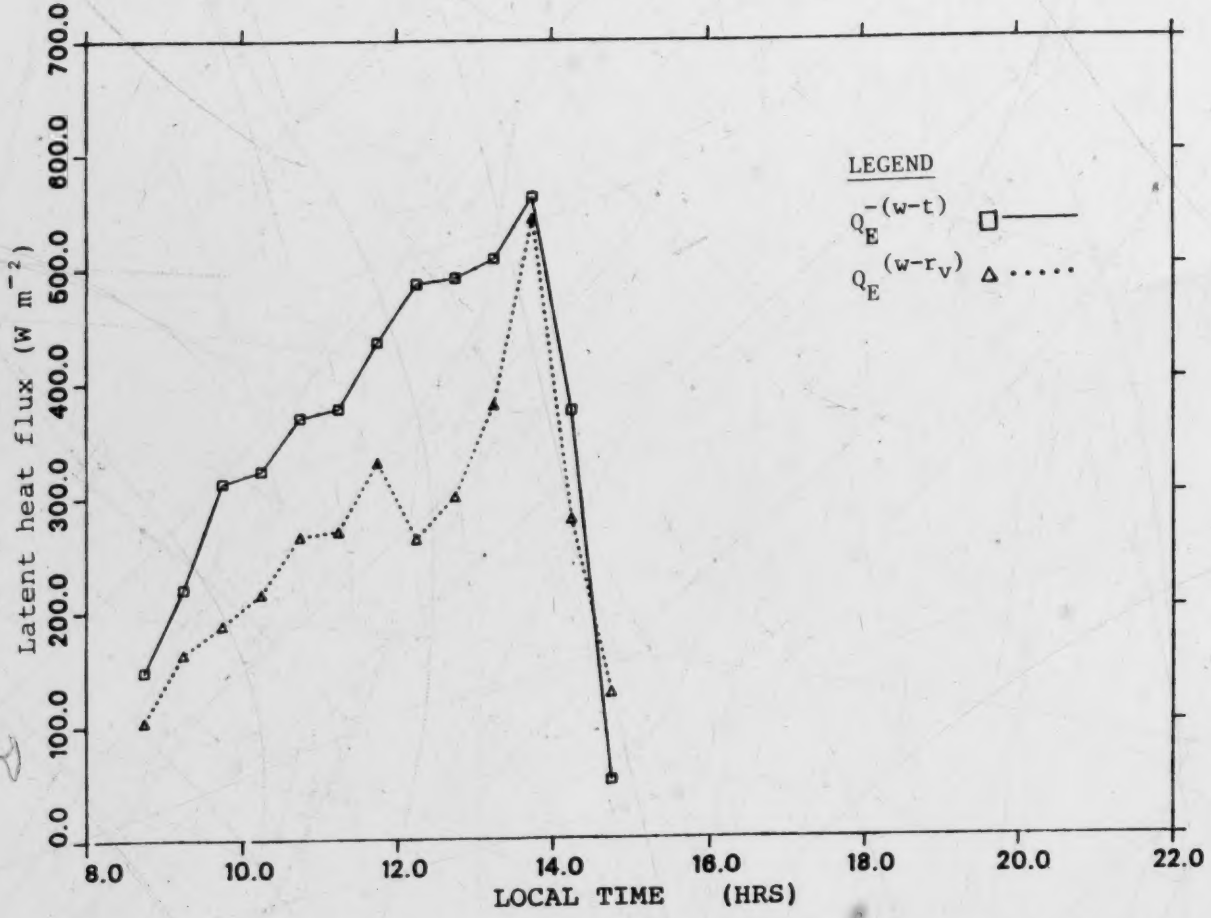

Figure 26. Comparative latent heat fluxes for June 23, 1988.

$$Q_E^{BR} = \frac{Q^* - Q_G}{B + 1} \qquad (27)$$

The first two methods are shown on each one of this set of figures with the third method being shown additionally on figures 24 and 25. This set of graphs is central to the purpose of this research as it compares the latent heat fluxes and therefore the evapotranspiration as given by our three methods. Ideally, if our instruments were all perfect, then all three would give the same values. Note that $Q_E^{(w-t)}$ almost always gave values greater than $Q_E^{(w-r_v)}$ and that this difference was generally greatest in the morning. The energy balances indicated a general loss of total energy as detected by the eddy correlation methods. The simplest hypothesis was that $Q_E^{(w-r_v)}$ was consistently too small.

The Bowen ratio equipment was only used on June 2 and June 14. Figures 24 and 25 show the results of these days coplotted with the 4.11 metre windspeed.

3.3. Discussion of the Failure to Close the Energy Balance

If $L\overline{w\rho}_v + \rho C_p \overline{wT} < Q^* - Q_G$, then either the radiometer has read too high (considered unlikely because it was new and factory calibrated) or one or both eddy correlation fluxes is too small. The eddy flux determinations share the same w signal, and since the thermocouple

is a simple measurement, it is natural to suspect the Lyman-α and sonic anemometer determinations. An estimate of the error in the soil heat flux measurement follows in Section 3.4.

The sonic anemometer velocity signal can be in error due to probe-induced flow distortion; in addition it is incapable of measuring eddy contributions below a certain size and above a certain frequency so that some signal loss is expected. The wind flow across the sonic could be disturbed by the Lyman-α humidiometer, which was mounted only 10 cm from the velocity measurement path. This separation was later increased to 20 cm but no notable change in the overall energy flux was observed. Thus the flow distortion was likely not the problem.

As for the possibility of flux loss due to unresolved eddies, we follow Kaimal (1972). Kaimal found that the highest frequency component contributing to the eddy flux is approximately $f = 10\ u/z$. Given that the height of the sonic anemometer was about 2 metres and that the maximum winds at that height were about 5 m/s, this equation suggests a maximum contributing frequency of 25 Hz, far below the 78 Hz measurement frequency of the CA27. The corresponding minimum significant wavelength for vapour transport in this flow would be about $\lambda_{min} = u/f_{max} \cong 20$ cm. Since the spacing between the two sonic transducers is 10 cm and the velocity path to

scalar-sensor spacing was about 20 cm, we would expect negligible loss of flux due to sensor separation and path averaging.

Another possibility which would account for the larger loss of energy in the morning was investigated: it was suspected that the drifting reference temperature at the base of the sonic anemometer arm was inducing an error in the temperature fluctuation signal. To investigate this possibility, the instrumentation was altered on June 14 to compare the sensible heat flux as determined from the relative temperature fluctuation with that obtained from the absolute temperature fluctuation. This was done by inserting an additional thermocouple into the reference point on the sonic anemometer. The results of this trial follow on Figure 27. No significant difference was noted.

The known sources of error for the sonic anemometer have been ruled out leaving the likelihood of a poor measurement of the fluctuating humidity by the Lyman-α humidiometer.

The Bowen ratio gear should give further evidence for this conclusion. On June 2, when the agreement between $L\overline{w\rho_v} + \rho C_p \overline{wT}$ and $Q^* - Q_G$ was fairly good, the Bowen ratio equipment agreed quite well with $L\overline{w\rho_v}$. On June 14 the direct fluxes seriously under-estimated $Q^* - Q_G$ from about 1130 to 1630. Several Bowen ratio measurements

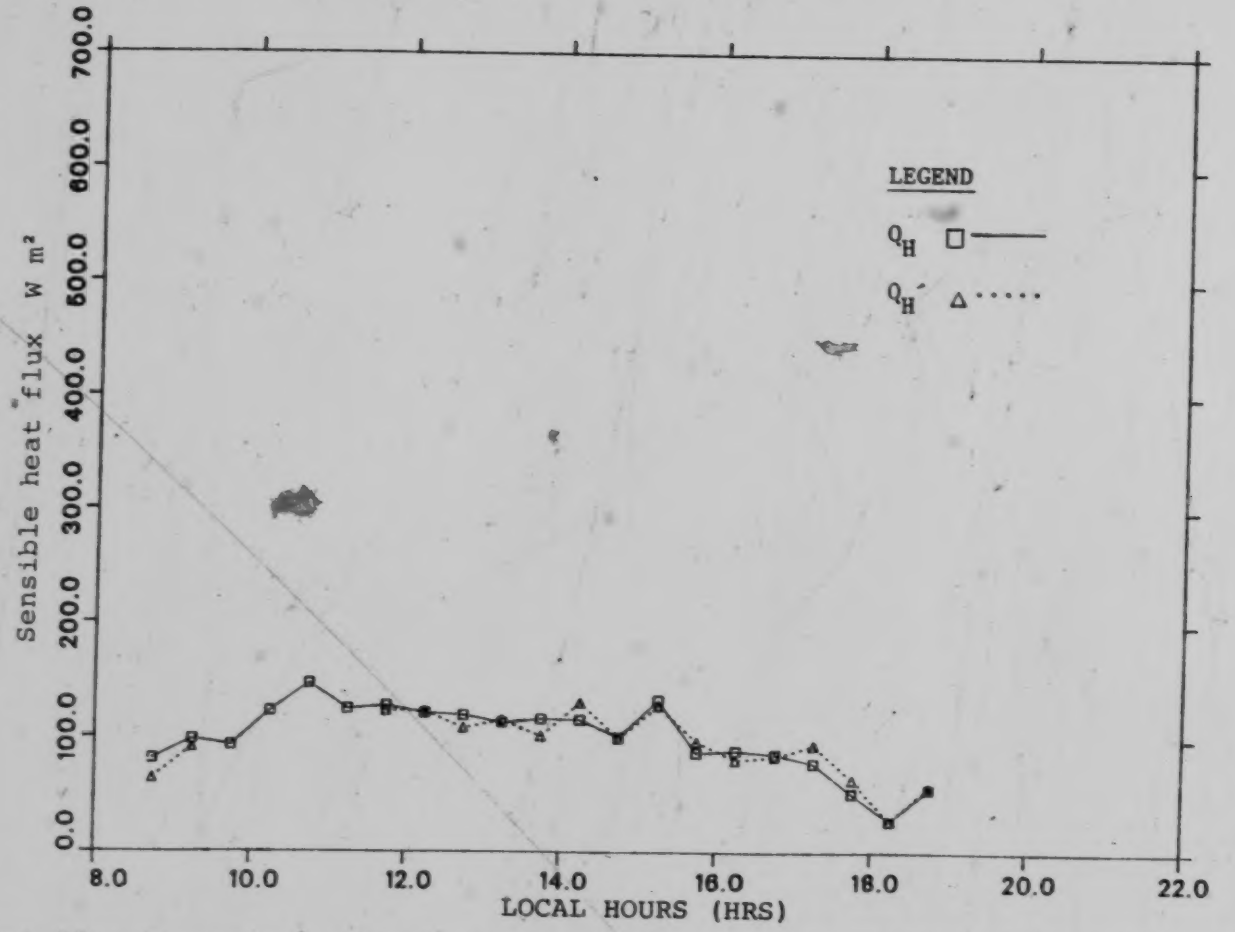

Figure 27. Comparison of sensible heat fluxes using relative temperature fluctuations Q_H and absolute temperature fluctuations Q_H' for June 14, 1988.

during this period disagree seriously with the direct latent heat flux $L\overline{w\rho_v}$, suggesting that the latter was in error. The evidence given by the Bowen ratio equipment was therefore ambiguous in evaluating our conclusion. In addition, on June 14 when the arm was placed horizontally in the field to check for offsets between the psychrometers, an error of 0.04 K was being shown in the dry bulb temperatures with typical signals being about 0.5 K. Table 2 gives details of the results of two consecutive 15-minute periods with the device horizontal. With this error observed it was decided that the data were not reliable enough to determine the accuracy of the other two methods and its use was discontinued.

Table 2. Results of horizontal measurements with Bowen ratio device for June 14, 1988.

	Period A	Period B
ΔT	-0.035	0.048
ΔT_w	-0.077	-0.096
Δe	-8.518	-16.14
$\Delta e/\gamma$	-0.139	-0.263

Table 2 implies an estimated typical mid-day error of 25 percent which is too large. The Bowen ratio equipment was suspected to be suffering from radiation error.

3.4. Estimate of Soil Heat Flux Error

The soil heat flux plate was buried under 5 cm of soil. No correction or measurement was attempted in the field to determine the amount of heat being gained or lost in the layer above the plate. Normally, by day, the soil above the plate will absorb incoming energy and warm in the process. This would suggest that the soil heat flux measured at the plate is generally under-estimated by day.

Following Sellers (1965) we can obtain an estimate of this error. Sellers found that the soil heat flux varied with time and depth according to:

$$\frac{Q_G(z,t)}{Q_G(0,t)} = e^{-z(\omega/2\kappa)^{\frac{1}{2}}} \frac{\sin[\omega t - (\omega/2\kappa)^{\frac{1}{2}} z + \pi/4]}{\sin(\omega t + \pi/4)} \qquad (28)$$

where e is the base of the natural logarithms, ω is the frequency (in this case, diurnal), and κ is the soil diffusivity.

The damping depth, D, is defined by

$$D = (2\kappa/\omega)^{\frac{1}{2}} \qquad (29)$$

and the amplitude reduction factor is given by $e^{-z/D}$.

The black chernozemic soil at the field would have diffusivity values ranging roughly from 10^{-7} m^2/s dry to 10^{-6} m^2/s wet (oke, 1978). This implies a daily damping depth range of from 5 cm dry to 17 cm wet.

The amplitude reduction at 5 cm would then range from 0.37 dry to 0.75 wet.

The maximum soil heat fluxes at plate depth were measured to be approximately 32 W/m^2. This, combined with the above amplitude reduction factor, suggests that the maximum error due to soil heat storage would be approximately 20 W/m^2.

3.5. Canopy Resistance

The canopy resistances inferred from this instrumentation are shown on figures 28 to 35. The canopy resistance was estimated using Equation (14) as previously shown in Chapter I. Both the latent and sensible heat flux values were directly from the eddy correlations in all these cases. The Bowen ratio gear data were not used for this purpose.

All these calculations had to be carried out for the height of the psychrometer which was being used to calculate the vapour pressure deficit (compared to saturation). The wind speed at the psychrometer height was determined using a least squares fit to the log wind profile of the windspeeds at the three anemometers. With the wind speed known it was possible to solve for the friction velocity which is related to the slope of the wind profile by von Karman's constant. The aerodynamic resistance is then found using Thom's Equation (11) from

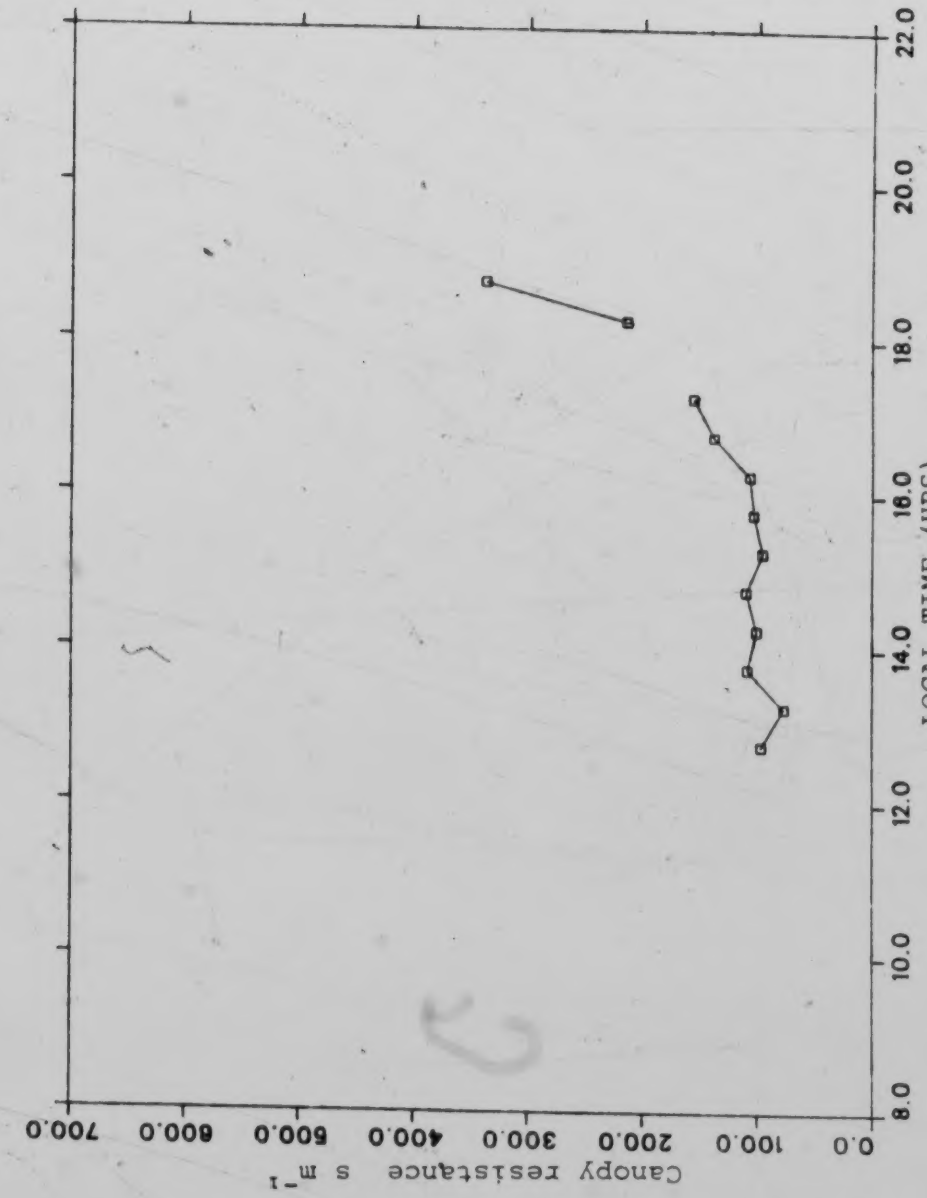

Figure 28. Canopy resistances for May 15, 1988.

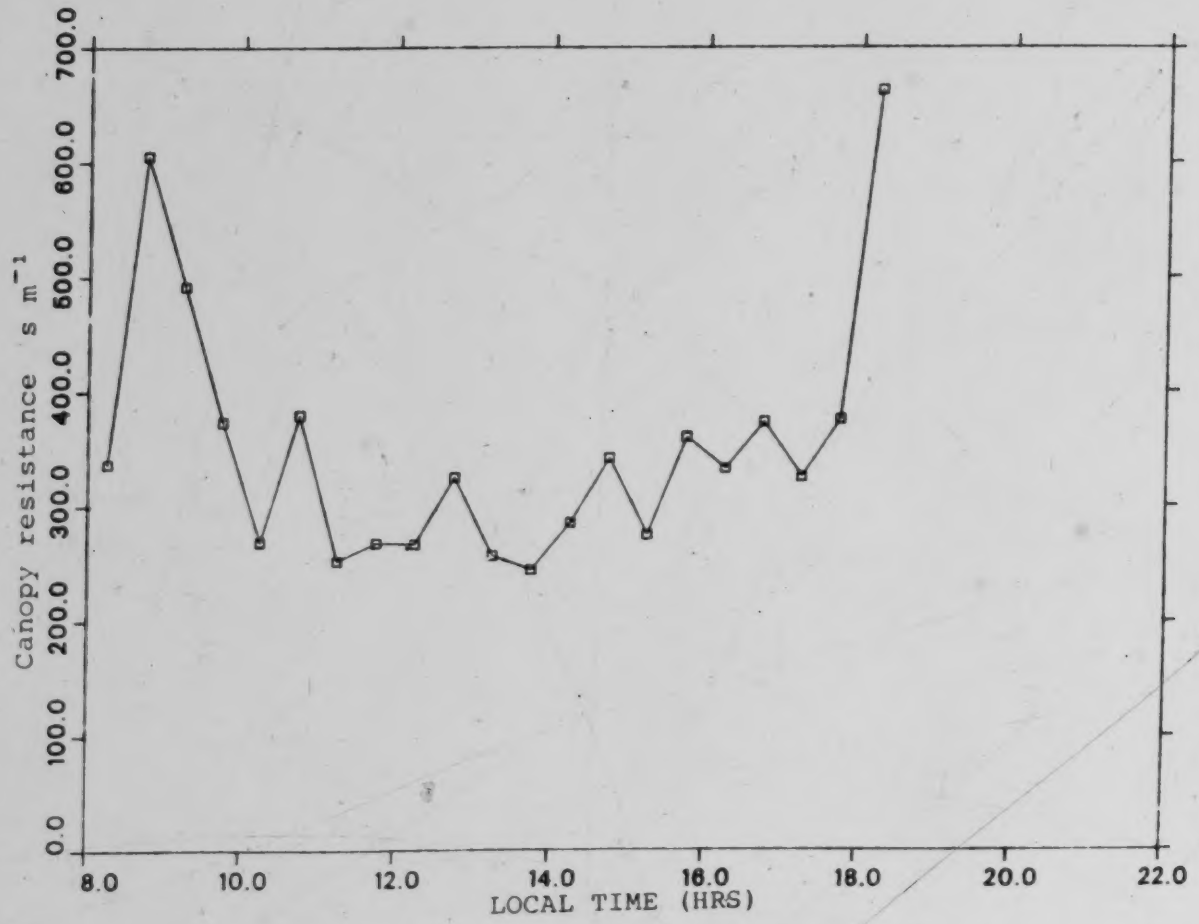

Figure 29. Canopy resistances for May 16, 1988.

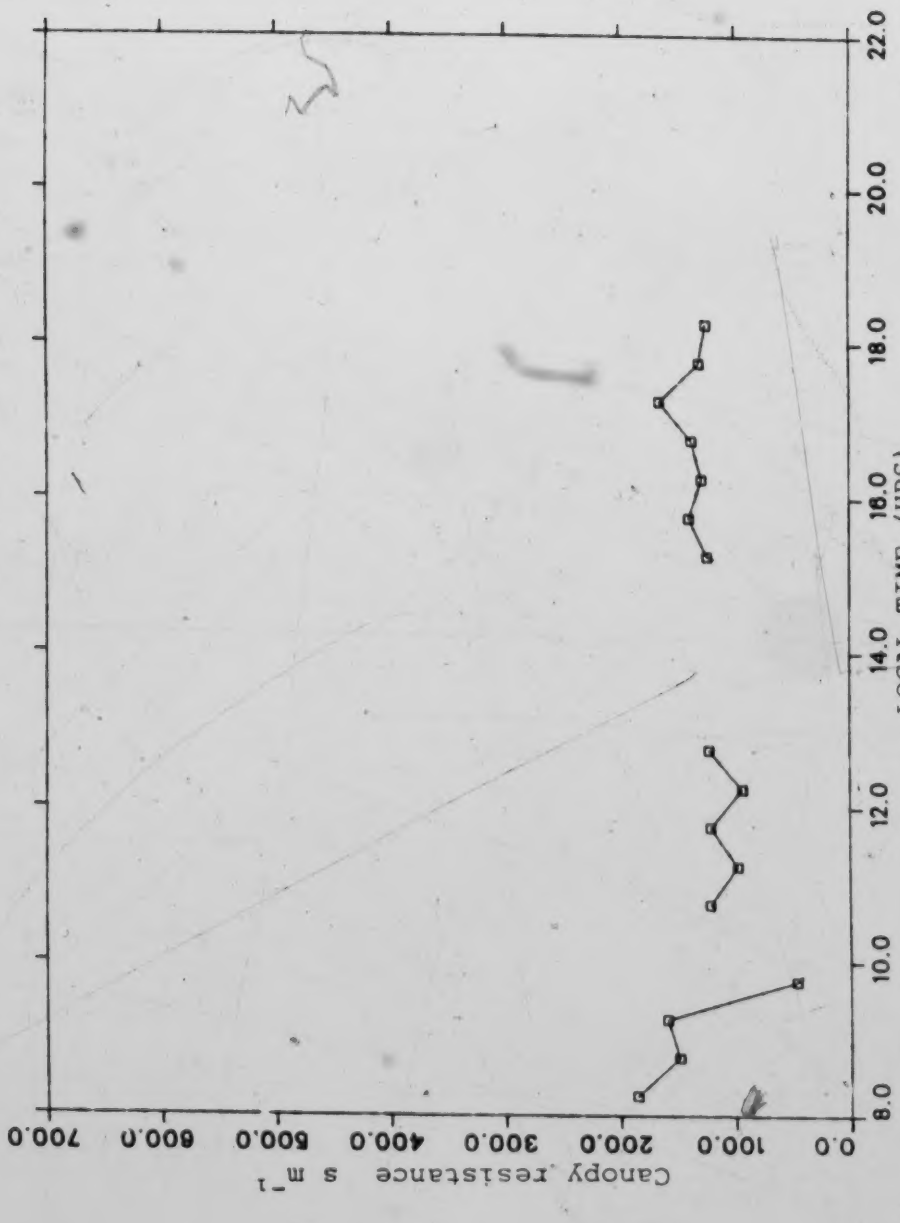

Figure 30. Canopy resistances for May 17, 1988.

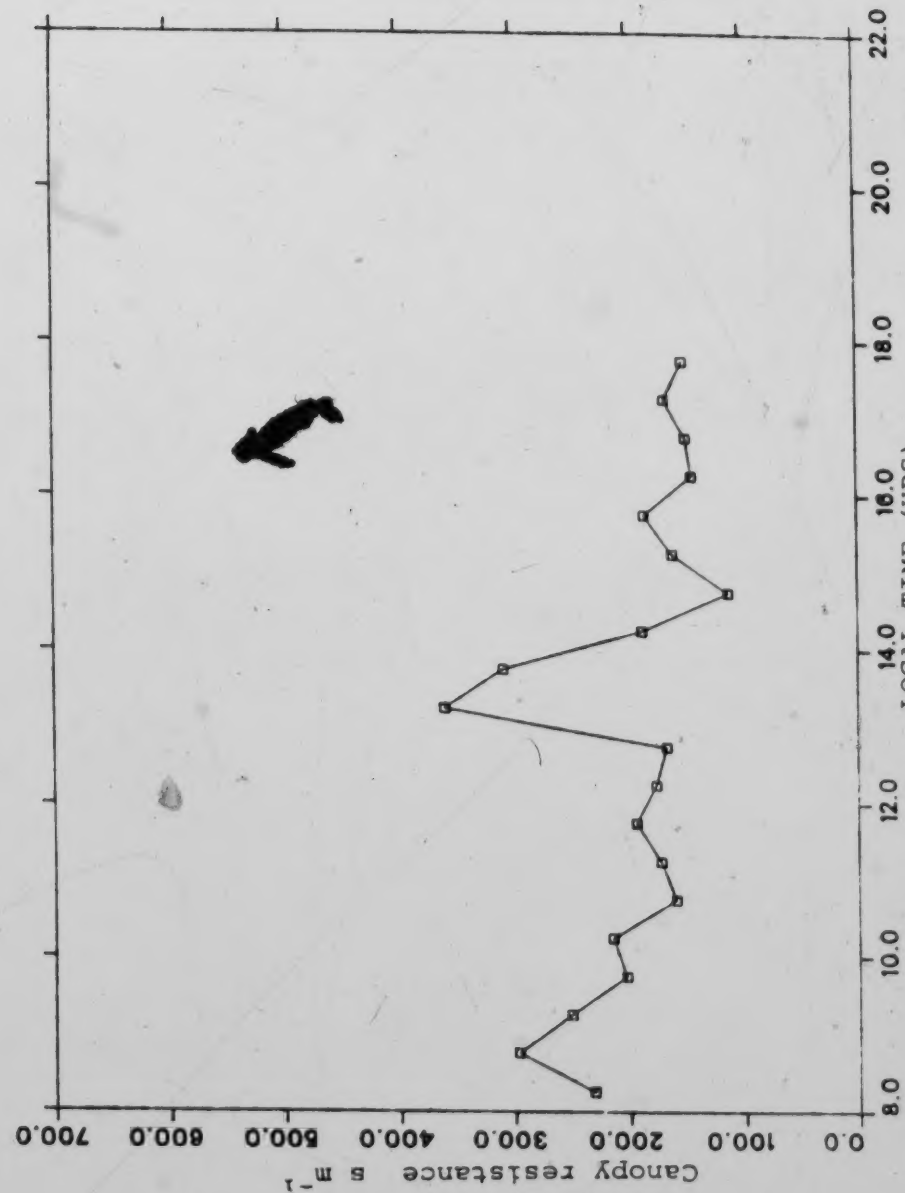

Figure 31. Canopy resistances for May 18, 1988.

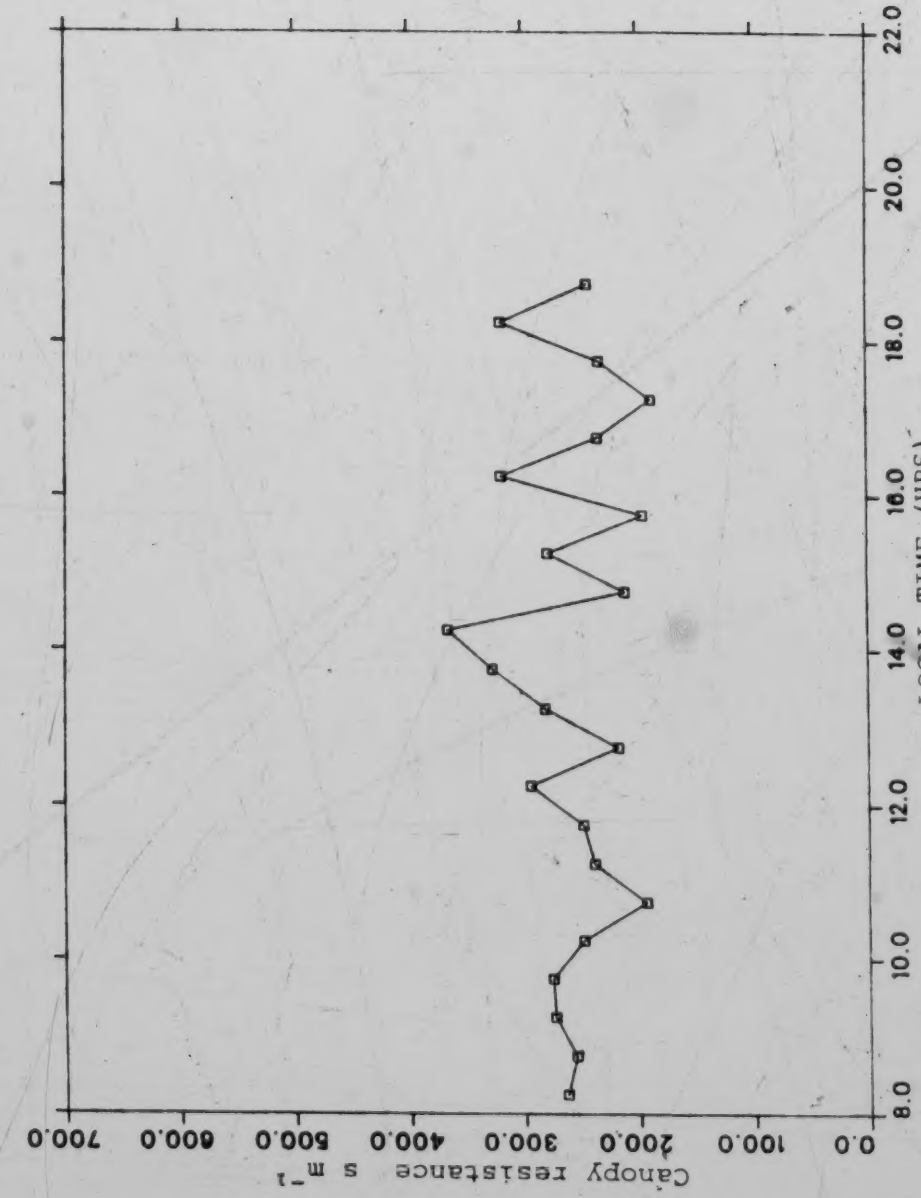

Figure 32. Canopy resistances for May 19, 1988.

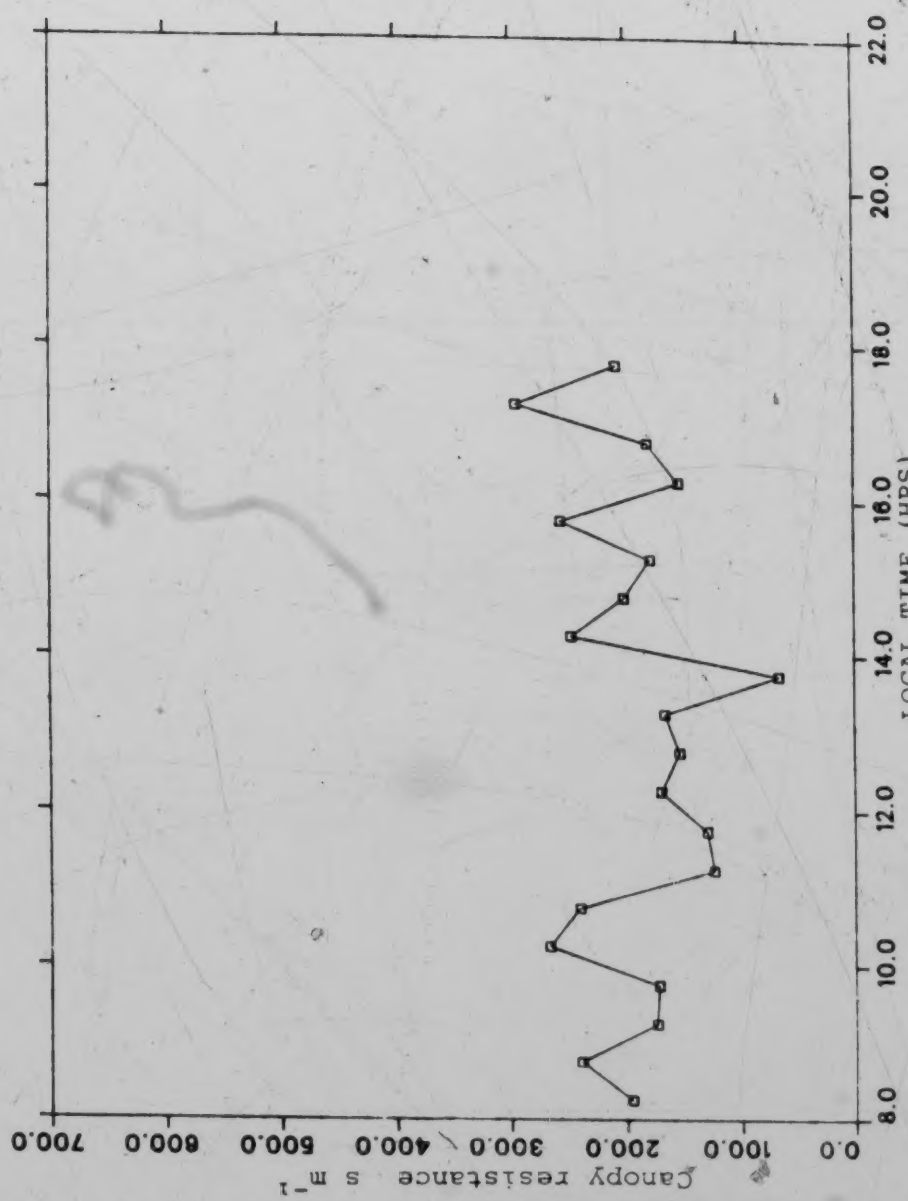

Figure 33. Canopy resistances for May 20, 1988.

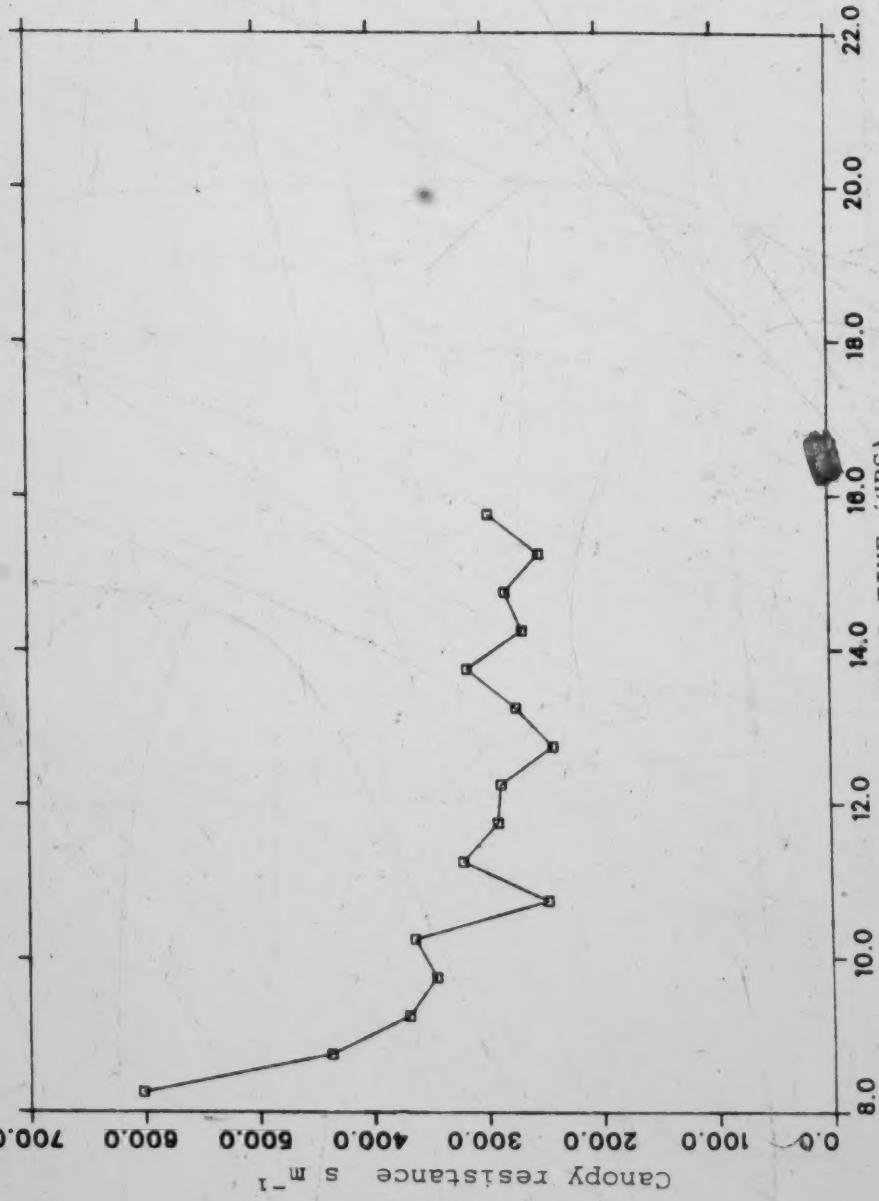

Figure 34. Canopy resistances for May 21, 1988.

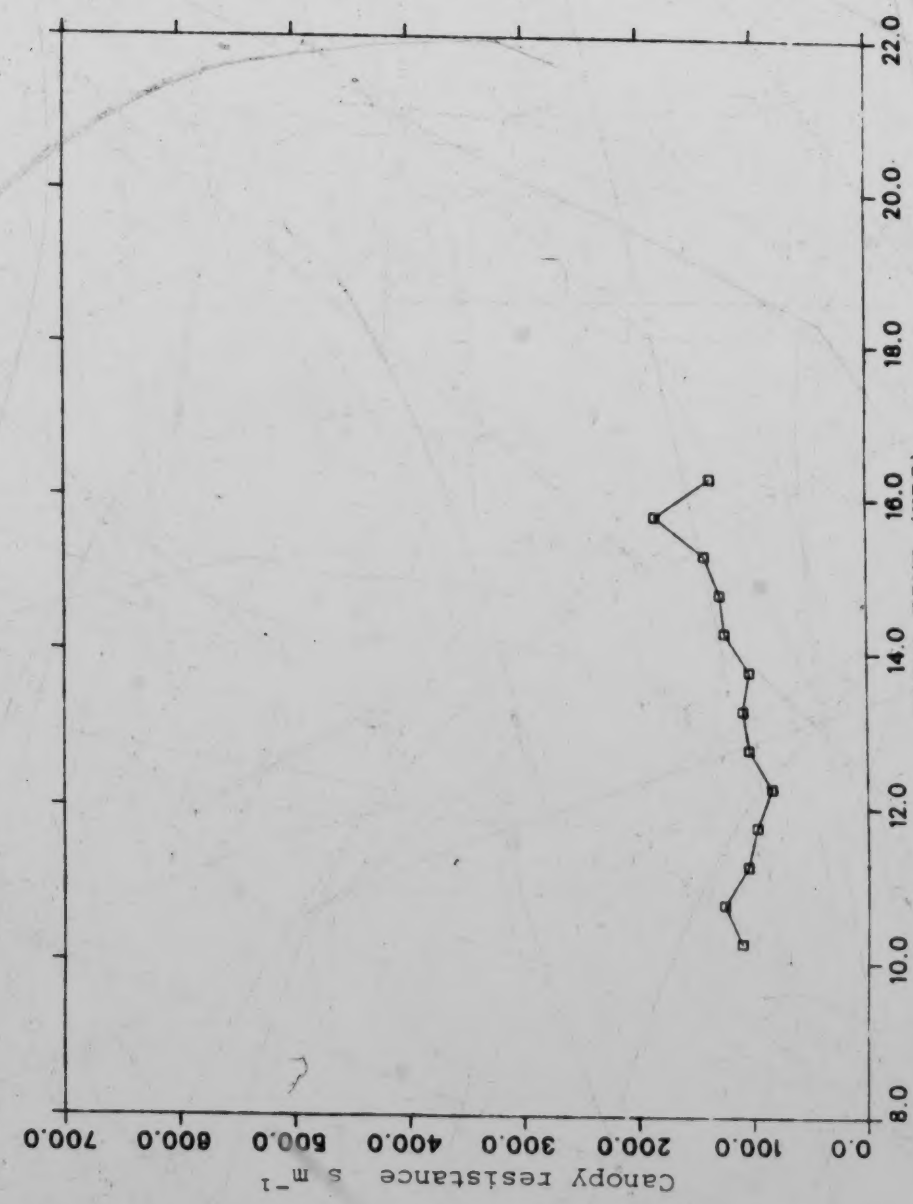

Figure 35. Canopy resistances for June 2, 1988.

Chapter I. An example of a plot of the aerodynamic resistance as determined from our wind profiles is shown on Figure 36 along with the 4.11 metre windspeed. These values were found to vary inversely with the wind speed as expected. That is, high wind speeds corresponded with lower r_a values.

The estimated canopy resistances averaged approximately 200 s/m and were higher than a previous study by Russell (1978). Russell found that the value of the resistance over fields of barley and pasture averaged around 80 s/m. Russell's study was carried out during conditions of much greater moisture, favouring lower canopy resistances. The expected diurnal trend towards high resistances in the early morning or late evening are shown in figures 28, 29, and 34. Note from Table 1 that conditions were quite dry for most of the May period of the field season so that fairly high resistances would be expected at those times and were observed. The exception to this was when the crop was moist with dew or shortly after a rainfall such as occurred on May 17. Appendix 2 gives a brief description of the field conditions for each plotted day of data.

Table 1 gives a summary of the total rainfall (R_t), daily average Bowen ratios (BR), mid-day canopy resistances (r_c), and temperatures (T) for each day for which they were measured. In general both the Bowen ratio

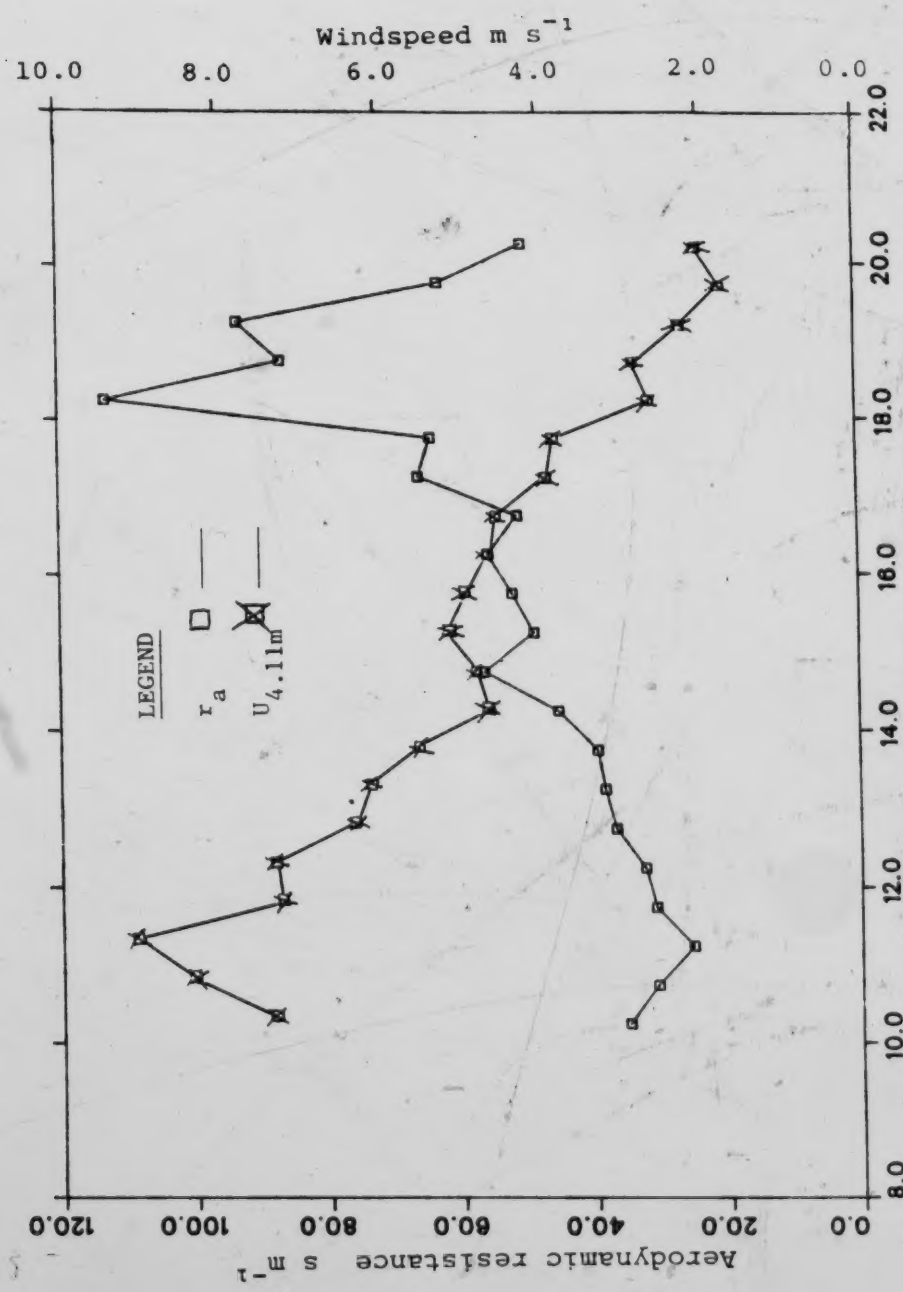

Figure 36. Aerodynamic resistances for June 2, 1988.

and the canopy resistance tend towards lower values during conditions of greater moisture. Appendix 2 gives the wind and cloudiness conditions for each field day.

Canopy resistances for each field day versus total daily precipitation are given in Figure 37. The figure shows the large day-to-day changes that occurred in the canopy resistance values. The lower values correspond to conditions with more moisture, such as a heavy dew or rainfall. The rainfall on May 14 contributed to the low canopy resistance on May 15 as did the trace of rain on May 17, with lower values for that day as well.

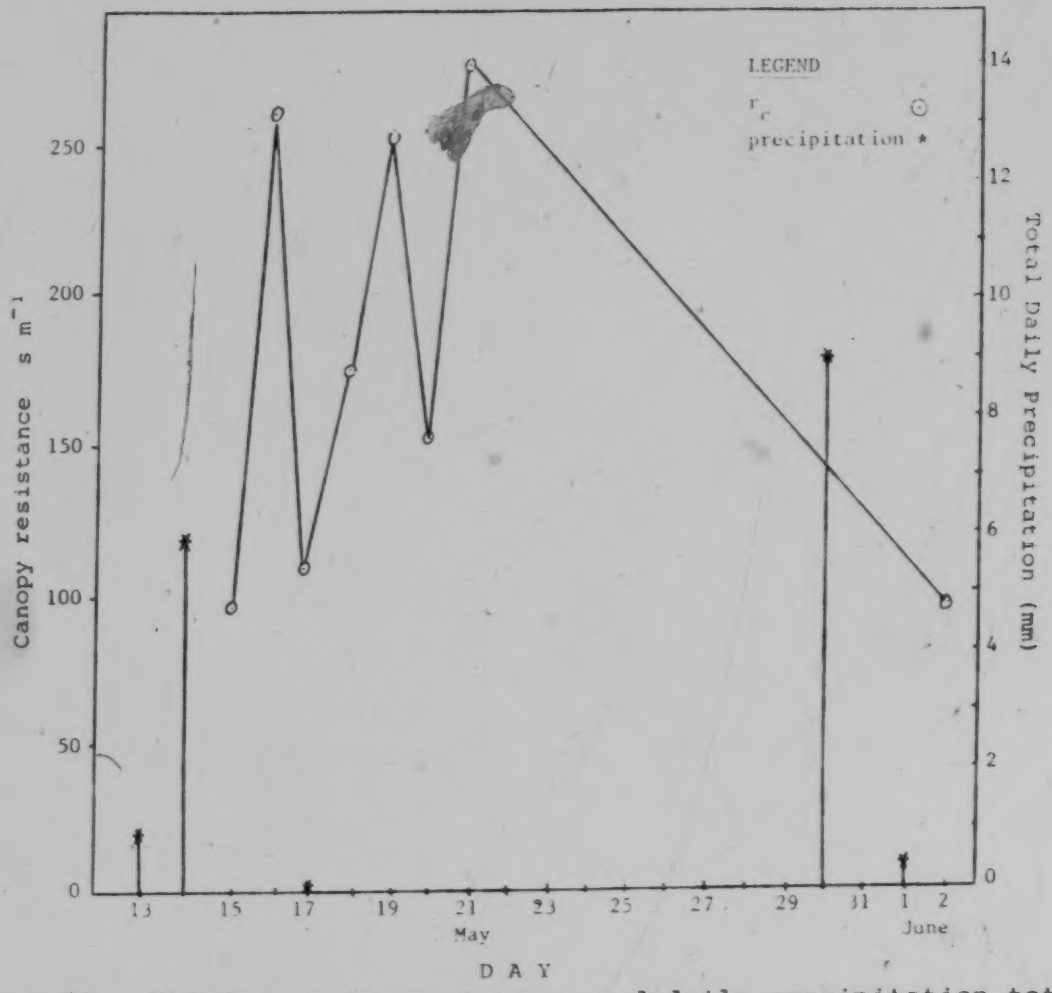

Figure 37. Mid-day canopy resistance and daily precipitation totals.

CHAPTER IV

CONCLUSIONS

Both eddy correlation methods were capable of giving reasonable energy balances but neither was consistently equivalent to the total flux suggested by the net radiometer less the soil heat flux, especially in the morning.

The Lyman-α humidiometer was suspected as the most likely to be causing a loss of flux. This conclusion was largely reached by a process of elimination that investigated all reasonable sources of error for the sonic anemometer.

The reversing psychrometer device was used for only two days, and although it gave results that were generally consistent with the other two methods, its field performance was not adequate to allow it to be the "tie breaker" to determine which of the eddy correlation methods was more accurate.

The canopy resistances obtained from this instrumentation were generally between 100 and 300 s/m. A

diurnal trend was noted on some days and the values generally varied as expected in reaction to ambient moisture conditions. Even with the errors inherent to the instruments used to calculate this parameter it is likely that these values were closer to the true values than any textbook values chosen for such crops (for lack of any measured data). It is therefore possible that these values will be of interest to agronomists and drought researchers.

BIBLIOGRAPHY

Bailey, W.G. and J.A. Davies, 1981a: The effect of uncertainty in aerodynamic resistance on evaporation estimates from the combination model. Boundary-Layer Meteorology, 20, 187-199.

Bailey, W.G. and J.A. Davies, 1981b: Bulk stomatal resistance control on evaporation. Boundary-Layer Meteorology, 20, 401-415.

Bailey, W.G. and J.A. Davies, 1981c: Evaporation from soybeans. Boundary-Layer Meteorology, 20, 417-428.

Black, T.A. and K.G. McNaughton, 1971: Psychrometric apparatus for Bowen ratio determination over forests. Boundary-Layer Meteorology, 2, 246-254.

Black, T.A. and K.G. McNaughton, 1972: Average Bowen ratio methods of calculating evapotranspiration applied to a Douglas fir forest. Boundary-Layer Meteorology, 2, 466-475.

Broersma, K., A.L. van Ryswyk, and R.J. Williams, 1978: Equilibrium and actual evapotranspiration from very dry vegetated surfaces. Journal of Applied Meteorology, 17, 1827-1832.

Davies, J.A. and C.D. Allen, 1973: Equilibrium, potential and actual evaporation from cropped surfaces in southern Ontario. Journal of Applied Meteorology, 12, 649-657.

Grant, D.R., 1975: Comparison of evaporation measurements using different methods. Quarterly Journal of the Royal Meteorological Society, 101, 543-550.

Kaimal, J.C., J.C. Wyngaard, Y. Izumi, and O.R. Cote, 1972: Spectral characteristics of surface-layer turbulence. Quarterly Journal of the Royal Meteorological Society, 98, 563-589.

Monteith, J.L., 1965: Evaporation and environment. In: G.F. Fogg (ed.) "The state and movement of water in living organisms", Academic Press, New York, 205-234.

Monteith, J.L., 1981: Evaporation and surface temperature. Quarterly Journal of the Royal Meteorological Society, 107, 1-27.

Noat, O. and Y. Mahrer, 1989: Modeling microclimate environments: a verification study. Boundary-Layer Meteorology, 46, 333-354.

Oke, T.R., 1978: Boundary Layer Climates. Methuen, New York.

Russell, G., 1980: Crop evaporation, surface resistance and soil water status. Agricultural Meteorology, 21, 213-226.

Rutter, A.J., 1972: Transpiration. Oxford University Press, London.

Sargeant, D.H. and C.B. Tanner, 1967: A simple psychrometric apparatus for Bowen ratio determinations. Journal of Applied Meteorology, 6, 414-418.

Sellers, W.D., 1965: Physical climatology. University of Chicago Press, Chicago.

Shuttleworth, W.J., 1976: A one-dimensional theoretical description of the vegetation atmosphere interaction. Boundary-Layer Meteorology, 10, 273-302.

Shuttleworth, W.J., 1978: A simplified one-dimensional theoretical description of the vegetation atmosphere interaction. Boundary-Layer Meteorology, 14, 3-27.

Shuttleworth, W.J., 1979: Below canopy fluxes in a simplified one-dimensional theoretical description of the vegetation atmosphere interaction. Boundary-Layer Meteorology, 17, 315-331.

Shuttleworth, W.J. and J.S. Wallace, 1985: Evaporation from sparse crops: an energy combination theory. Quarterly Journal of the Royal Meteorological Society, 111, 839-855.

Spittlehouse, D.L. and T.A. Black, 1982: A comparison of reversing psychrometric Bowen ratio measurement systems. Atmosphere-Ocean, 372-379.

Thom, A.S., 1972: Momentum, mass and heat exchange of vegetation. Quarterly Journal of the Royal Meteorological Society, 98, 124-134.

Van Zyl, W.H. and J.M. De Jager, 1987: Accuracy of the Penman-Monteith equation adjusted for atmospheric stability. Agricultural and Forestry Meteorology, 41, 57-64.

APPENDIX 1

DETAILS OF CR21X OPERATION FOR THIS FIELD SEASON

I. CR21X input configuration used with this program.

A. Single ended input locations

1. soil heat flux plate
2. net radiometer
3. sonic anemometer
4. fine wire thermocouple
5. Lyman-α

B. Differential input locations

6. psychrometer total voltage drop across two diodes
7. psychrometer dry bulb diode voltage drop

C. Pulse input locations

1. low anemometer
2. middle anemometer
3. high anemometer

II. Input storage locations

1. soil heat flux
2. net radiation
3. vertical velocity
4. temperature fluctuation
5. Lyman-α voltage
6. log Lyman-α voltage
7. log Lyman-α voltage minus mean log Lyman-α voltage

8. location 7 multiplied by slope of Lyman-α graph
9. wT
10. w^2
11. T^2
12. ρ_v
13. $w\rho_v$
14. $\rho_v{}^2$
15. unused
16. unused
17. mean absolute humidity
18. log mean Lyman-α voltage
19. slope of Lyman-α curve
20. unused
21. low anemometer
22. middle anemometer
23. high anemometer
24. total psychrometer voltage
25. dry bulb psychrometer voltage
26. unused
27. unused
28. CR21X battery voltage

III. Output storage locations

1. unused
2. date
3. time
4. soil heat flux
5. net radiation
6. $\overline{w}$
7. $\overline{T}$
8. mean Lyman-α voltage
9. mean log Lyman-α voltage
10. $\overline{wT}$

11. $\overline{w^2}$
12. $\overline{T^2}$
13. $\overline{\rho_v}$
14. $\overline{w\rho_v}$
15. $\overline{\rho_v^2}$
16. mean total psychrometer voltage
17. mean psychrometer dry bulb voltage

IV. CR21X program used for field program

CR21X Program Code							Function
A. SAMPLING							
P10	28						Battery voltage (21X)
P1	1	1	1	1	2500	0	Q_G W m^{-2}
P1	1	4	2	2	10.1	0	Q* W m^{-2}
P1	1	5	3	3	.001	0	sonic w m s^{-1}
P1	1	5	4	4	.004	0	sonic T °C
P1	1	5	5	5	.001	0	Lyman-α volts
P2	2	4	6	24	1	0	Psychrometer
B. PROCESSING							
P30	_____		17				stores mean humidity
P30	_____		18				stores Lyman-α voltage
P30	_____		19				stores Lyman-α curve slope
P36	3	4	9				calculates wT
P36	3	3	10				calculates w^2
P36	4	4	11				calculates T^2
P40	5	6					calculates ln Lyman-α voltage
P35	6	18	7				(ln Lyman-α mean ln Lyman-α) volts
P36	7	19	8				calculates
P33	8	17	12				calculates ρ_v
P36	12	3	13				calculates $w\rho_v$
P36	12	12	14				calculates ρ_v^2

CR21X Program Code — Function

C. OUTPUT

```
P92    0    30    10
P77  110
P71    6     1
P71    6     9
P71    2    24
```

D. TABLE 2 FOR ANEMOMETERS

```
P03    3     1   10   21   0.025   0.25
P92    0    30   10
P71    3    21
```

Note: Storage locations in section B with blank lines indicate where values were input manually according to daily conditions.

APPENDIX 2

DAILY CONDITIONS DURING FIELD SEASON

May 15:	sky clear, light west wind, crop slightly damp
May 16:	sky clear, cool, light south wind
May 17:	cloudy, cool, strong northwest winds, brief period of very light rain, some afternoon sunny breaks
May 18:	partly cloudy, northwest wind, cool
May 19:	clear, cool, light southwest winds becoming northwesterly in the afternoon, a few clouds after mid-day
May 20:	sunny, cool, moderate northwest wind
May 21:	sunny, warm, dry, light southerly breeze, heavy dew in the morning
June 2:	sunny, cool, moderate west to northwest breeze, vegetation beginning to develop
June 14:	sunny, cool, light west wind, vegetation much thicker than on previous day, road machines at work on nearby upwind road
June 15:	sunny, cool, moderate south wind, high cloud in afternoon
June 23:	high cloud, wet surface, light west to northwest wind, thunderstorm ends day early